# Inhibition of the epigenetic suppressor EZH2 primes osteogenic differentiation mediated by BMP2

Received for publication, October 29, 2019, and in revised form, April 22, 2020 Published, Papers in Press, April 24, 2020, DOI 10.1074/jbc.RA119.011685

**Amel Dudakovic[1,2], Rebekah M. Samsonraj[1], Christopher R. Paradise[3,4], Catalina Galeano-Garces[1], Merel O. Mol[5], Daniela Galeano-Garces[1], Pengfei Zan[1,6,7], M. Lizeth Galvan[1], Mario Hevesi[1], Oksana Pichurin[1], Roman Thaler[1], Dana L. Begun[1], Peter Kloen[5], Marcel Karperien[8], A. Noelle Larson[1], Jennifer J. Westendorf[1,2], Simon M. Cool[9,10], and Andre J. van Wijnen[1,2,*]**

*From the [1]Department of Orthopedic Surgery, Mayo Clinic, Rochester, Minnesota, USA, [2]Department of Biochemistry & Molecular Biology, Mayo Clinic, Rochester, Minnesota, USA, [3]Mayo Clinic Graduate School of Biomedical Sciences, Mayo Clinic, Rochester, Minnesota, USA, [4]Center for Regenerative Medicine, Mayo Clinic, Rochester, Minnesota, USA, [5]Department of Orthopedic Surgery, Amsterdam University Medical Center, Amsterdam, The Netherlands, [6]Department of Orthopedic Surgery, School of Medicine, Second Affiliated Hospital of Zhejiang University, Hangzhou, China, [7]Department of Orthopedic Surgery, School of Medicine, Shanghai Tenth People's Hospital Affiliated to Tongji University, Shanghai, China, [8]Department of Developmental BioEngineering, University of Twente, Enschede, The Netherlands, [9]Glycotherapeutics Group, Institute of Medical Biology, Agency for Science, Technology and Research (A*STAR), Singapore, and [10]Department of Orthopaedic Surgery, Yong Loo Lin School of Medicine, National University of Singapore, Singapore*

Edited by John M. Denu

**Bone-stimulatory therapeutics include bone morphogenetic proteins (*e.g.* BMP2), parathyroid hormone, and antibody-based suppression of WNT antagonists. Inhibition of the epigenetic enzyme enhancer of zeste homolog 2 (EZH2) is both bone anabolic and osteoprotective. EZH2 inhibition stimulates key components of bone-stimulatory signaling pathways, including the BMP2 signaling cascade. Because of high costs and adverse effects associated with BMP2 use, here we investigated whether BMP2 dosing can be reduced by co-treatment with EZH2 inhibitors. Co-administration of BMP2 with the EZH2 inhibitor GSK126 enhanced differentiation of murine (MC3T3) osteoblasts, reflected by increased alkaline phosphatase activity, Alizarin Red staining, and expression of bone-related marker genes (*e.g.* Bglap and Phospho1). Strikingly, co-treatment with BMP2 (10 ng/ml) and GSK126 (5 $\mu$M) was synergistic and was as effective as 50 ng/ml BMP2 at inducing MC3T3 osteoblastogenesis. Similarly, the BMP2–GSK126 co-treatment stimulated osteogenic differentiation of human bone marrow–derived mesenchymal stem/stromal cells, reflected by induction of key osteogenic markers (*e.g.* Osterix/SP7 and IBSP). A combination of BMP2 (300 ng local) and GSK126 (5 $\mu$g local and 5 days of 50 mg/kg systemic) yielded more consistent bone healing than single treatments with either compound in a mouse calvarial critical-sized defect model according to results from $\mu$CT, histomorphometry, and surgical grading of qualitative X-rays. We conclude that EZH2 inhibition facilitates BMP2-mediated induction of osteogenic differentiation of progenitor cells and maturation of committed osteoblasts. We propose that epigenetic priming, coupled with bone anabolic agents, enhances osteogenesis and could be leveraged in therapeutic strategies to improve bone mass.**

This article contains supporting information.

* For correspondence: Andre J. van Wijnen, vanwijnen.andre@mayo.edu.

Bone morphogenetic proteins (BMPs) are protein ligands of the transforming growth factor superfamily of morphogens and growth factors that control many biological processes, including osteoblast differentiation and bone regeneration (1, 2). BMP2 is the first osteogenic member of this superfamily (3, 4) and one of the most widely studied and clinically relevant members of this protein family. BMP2 and BMP7 are potent inducers of bone formation *in vitro* and function by activating canonical BMP signaling via binding to types I and II BMP receptors (1, 5, 6). Activated BMP receptors then phosphorylate and activate Smad proteins (*e.g.* Smad1, 5, and 8), which in turn complex with a co-Smad (Smad4). These Smad complexes then translocate into the nucleus to induce transcriptional changes within activated cells (7). Runt-related transcription factor 2 (Runx2), the homeodomain transcription factor Dlx5, and the zinc finger protein Osterix/Sp7 are key genes induced by canonical BMP signaling (8–14). Transcriptional induction of Runx2 results in the activation of the osteogenic cascade in progenitor cells to stimulate osteoblast differentiation and bone formation (15).

Fracture healing is a regenerative process that recapitulates many of the events that occur during fetal stages of skeletal development (16, 17). Progenitor cells differentiate directly into osteoblasts during intramembranous bone repair whereas a cartilaginous callus precedes bone formation during endochondral bone repair. Osteogenic pathways, including BMP signaling, are critical for proper healing through both intramembranous and endochondral mechanisms (18). Although normal fracture healing results in complete bone restoration, 5 to 10% of all fractures do not heal properly (19–21) resulting in 100,000 nonunions each year in the United States (22). Delayed fracture healing can result in increased time lost from work and medical costs, chronic pain, opioid use, and disability. BMP proteins are induced during native fracture repair (23, 24) and their administration alone or in combination with carrier materials (*e.g.* col-

lagen sponge) has been shown to promote healing in fracture and critical-sized defect animal models (25–28). Following promising outcomes in clinical trials (29–31), BMP2 is in current clinical use for orthopedic indications including tibial fracture healing and high-risk spine fusion (32). Despite its success, the clinical applications of high concentrations of BMP2 are limited because of high cost (33) and detrimental side effects such as heterotopic ossification, osteolysis, and airway obstruction (2, 34). Thus, there is a need for safe augmentation of fracture healing and bone fusion in surgeries where there is a high risk of nonunion.

Epigenetic mechanisms are critical regulators of skeletal development and osteoblast differentiation (35–37). Enhancer of zeste homolog 2 (Ezh2), the catalytic subunit of the polycomb-repressive complex 2 (PRC2), catalyzes mono-, di-, and tri-methylation of lysine 27 of histone H3 (H3K27me1, H3K27me2, and H3K27me3) (38, 39). An alternative PRC2 complex in which Ezh1 serves as the catalytic subunit possesses the same enzymatic activity but appears to have a more restricted biological role (38, 40, 41). The enzymatic activity of the PRC2 complex and accumulation of the H3K27me3 mark is associated with chromatin condensation and gene suppression (38). Although Ezh2 is essential for proper skeletal patterning and bone formation (42–48), reducing the H3K27 methyltransferase activity of Ezh2 enhances osteogenic lineage commitment and osteoblast differentiation *in vitro*, as well as bone formation *in vivo* (44, 49–56). Mechanistically, Ezh2 loss results in a reduction in stem cell numbers and promotes expression of established bone-related genes, stimulates expression of genes involved in the activation of ligand-dependent signaling pathways (*e.g.* WNT, PTH, and BMP2 pathways), and enhances Smad1/5 phosphorylation (BMP2 signaling) in differentiating osteoblasts (44, 47, 54, 57). In a reciprocal manner, forced expression of Ezh2 inhibits *in vitro* and *in vivo* osteogenesis, highlighting the importance of Ezh2 in the osteogenic fate of stem cells (51).

Ezh2 inhibition may enhance bone-anabolic pathways in osteoblasts and be leveraged in clinical practice to promote biological bone repair. Because Ezh2 inhibitors such as GSK126 and EPZ-6438 have been assessed in clinical trials (58, 59), it may be feasible to combine these agents with BMP2 to enhance bone healing and reduce cost and side effects associated with BMP2. Therefore, in this study we assessed whether combining BMP2 treatment with Ezh2 inhibition would maximize osteogenic differentiation. We show that co-treatment of BMP2 and the Ezh2 inhibitor GSK126 promotes osteoblast differentiation *in vitro* and supports intramembranous bone healing in a critical-sized calvarial defect model *in vivo*.

## Results

### *Ezh2 inhibition synergizes with BMP2 to induce osteogenic differentiation of MC3T3 pre-osteoblasts*

Our group and others have shown that loss of Ezh2 function stimulates *in vitro* osteogenesis, enhances *in vivo* bone formation, and prevents bone loss associated with estrogen depletion (44, 51, 54–56). Additional analyses demonstrated that Ezh2 inhibition stimulates paracrine signaling, including activation

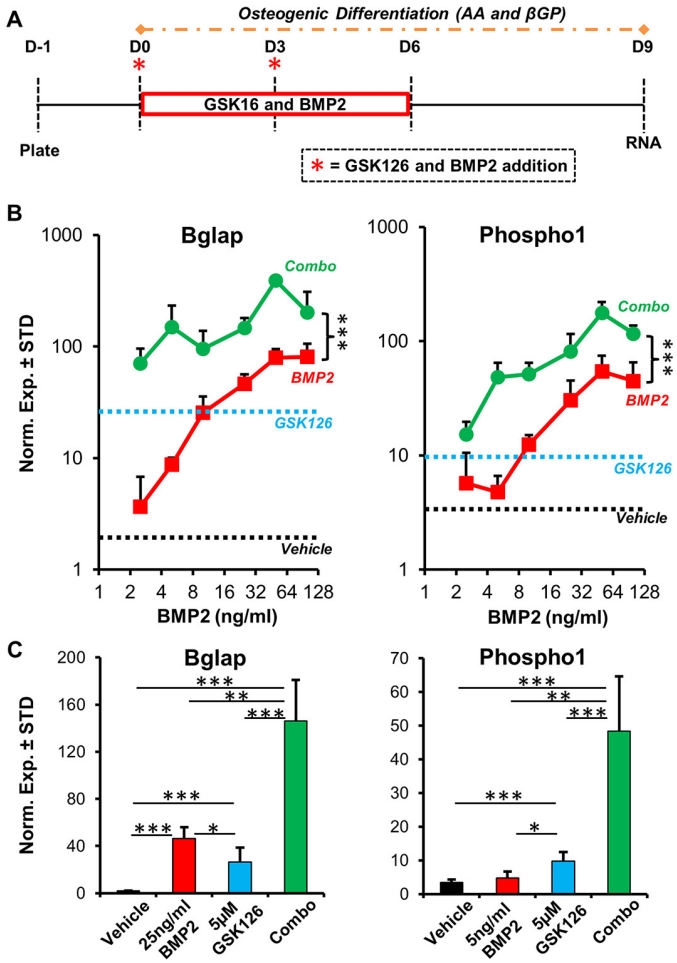


**Figure 1. GSK126 potentiates BMP2-induced expression of osteogenic genes in MC3T3 cells.** *A*, experimental set-up for BMP2 and GSK126 treatment and osteogenic differentiation of MC3T3 pre-osteoblasts. GSK126 and BMP2 were administered on days 0 and 3 of differentiation (cells were exposed to compounds for 6 days). RNA was isolated on day 9 of osteogenic differentiation. *B*, expression (RT-qPCR) of two established osteogenic markers, Bglap and Phospho1, on day 9 of differentiation ($n = 3$). Differentiating MC3T3 cells were treated with vehicle (*black dashed line*), 5 $\mu$M GSK126 (*blue dashed line*), varying concentrations of BMP2 (2.5 to 100 ng/ml) in the absence (*red solid line*) or presence (*green solid line*) of 5 $\mu$M GSK126. *C*, expression of Bglap and Phospho1 upon 5 $\mu$M GSK126 administration alone or in combination with and 25 ng/ml and 5 ng/ml BMP2, respectively ($n = 3$). * = $p < 0.05$, ** = $p < 0.01$, *** = $p < 0.001$.

of BMP signaling, enhanced expression of Wnt ligands, and up-regulation of the Pth1r receptor (54). To understand the interplay between osteoblast stimulatory effects of Ezh2 inhibition and the BMP signaling pathway, we assessed the impact of GSK126, a specific Ezh2 inhibitor, in combination with recombinant BMP2 during osteogenic differentiation of MC3T3 pre-osteoblasts (Fig. 1). Differentiating MC3T3 cells were treated with an established concentration of GSK126 (5 $\mu$M) (54) and varying concentrations of BMP2 (Fig. 1*A*). As demonstrated previously (44, 54), GSK126 enhances expression of osteoblast-related genes (osteocalcin/Bglap and phosphoethanolamine/phosphocholine phosphatase1/Phospho1) (Fig. 1*B* and Fig. S1). Similarly, BMP2 treatment also stimulates expression of these genes in a dose-dependent manner. Even the lowest concentration of BMP2 (2.5 ng/ml) enhances the expression of osteogenic genes. Maximal osteogenic gene expression is

reached with 50 ng/ml of BMP2 in MC3T3 cells. In this assay, 5 $\mu$M GSK126 is equivalent to 10 ng/ml BMP2 when comparing expression of Bglap and Phospho1 (Fig. 1*B*, compare *blue dashed line* with *red line*). Interestingly, when compared with BMP2 administration, the combination of 5 $\mu$M GSK126 with various BMP2 concentrations further stimulates osteogenic gene expression. It is noteworthy that low concentrations of BMP2 (2.5–10 ng/ml) in combination with GSK126 achieve expression levels similar to high BMP2 concentrations (Fig. 1*B*, compare *red line* to *green line*). Importantly, the combination of GSK126 and BMP2 exceeds the maximal effects of BMP2 alone on osteogenic gene expression. The effects of combinatory treatments are significantly different when compared with BMP2 treatment alone (Fig. 1*B*, *red versus green line*). As a further illustration of co-stimulatory effects, we compared gene expression at individual BMP2 concentrations (Fig. 1*C*). GSK126 and BMP2 enhance osteogenic gene expression; the dual administration of these pro-osteogenic factors synergistically activates Bglap and Phospho1 expression.

To further characterize this biological interaction between BMP2 and Ezh2 inhibition, GSK126 (5 $\mu$M) was combined with low (10 ng/ml) and high (50 ng/ml) concentrations of BMP2 in differentiating MC3T3 cells (Fig. 2*A*). As anticipated, both Ezh2 inhibition and BMP2 treatment stimulates expression of the key osteogenic transcription factor (Osterix/Sp7) and extracellular matrix genes (Bglap and bone sialoprotein/Ibsp) (Fig. 2*B*). Pairwise comparisons of each treatment group using two-way analysis of variation (ANOVA) demonstrates significantly different gene expression profiles throughout the differentiation time course for all three genes (Sp7, Bglap, and Ibsp) (Table S1). Of note, the combination of GSK126 and BMP2 (at both low and high concentrations) significantly enhances the effects of either agent alone. This is especially evident with the combination of GSK126 with the low BMP2 concentration (compare *dashed green line* to *blue* and *dashed red lines*). Expression profiles of Sp7, Bglap, and Ibsp for vehicle-treated samples are shown as individual line graphs (Fig. 2*C*), demonstrating that differentiation of MC3T3 cells enhances expression of osteogenic genes in the absence of BMP2 and GSK126. However, because the effects of BMP2 and GSK126 are rather dramatic, vehicle treatment under standard differentiation conditions in osteogenic media (*black line*) result in a far more modest up-regulation of osteogenic genes that is difficult to appreciate on a log scale. The synergistic effects of GSK126 and low BMP2 are evident when assessing Bglap and Ibsp expression on a single representative time point (day 6) during osteogenic differentiation (Fig. 2*D*). The gene expression data are corroborated by results obtained using assays detecting alkaline phosphatase activity (Fig. 2*E*) and Alizarin Red staining (Fig. 2*F*), which are established histochemical assays for osteoblast differentiation. Although minimal Alizarin Red staining is observed in low BMP2 and GSK126 treatment groups at this early stage of osteoblast differentiation, robust mineral deposition is observed with co-administration of GSK126 and low BMP2 on day 20 of osteoblastogenesis. Hence, our results demonstrate that inhibition of Ezh2 synergizes with BMP2 to stimulate differentiation of MC3T3 pre-osteoblasts.

### *Differential gene expression changes with Ezh2 inhibition and BMP2 administration*

To assess the mechanisms by which GSK126 and BMP2 co-stimulate osteoblast differentiation, RNA from differentiating MC3T3 cells (described in Fig. 2) was subjected to RNA-Seq analysis (Fig. 3). Unbiased principal component analysis (PCA) (60) of robustly expressed genes (RPKM >0.3 in at least one group per time point, $n$ = 11,974 genes on day 1, $n$ = 12,307 genes on day 6) reveals BMP2- and GSK126-specific clustering of gene expression profiles on day 1 (Fig. 3*A*) and day 6 (Fig. 3*B*). It is noteworthy that GSK126 plus BMP2 combination clusters differently when compared with each compound alone, suggesting distinct effects of these agents on gene expression in differentiating osteoblasts. Based on these findings, we set out to identify genes that are differentially expressed on day 1 and day 6 across the six different treatment groups (vehicle, 10 ng/ml BMP2, 50 ng/ml BMP2, 5 $\mu$M GSK126, 10 ng/ml BMP2 + 5 $\mu$M GSK126, and 50 ng/ml BMP2 + 5 $\mu$M GSK126). For this analysis, we selected genes that were detected by RNA-Seq (average RPKM >0.1 across six samples at each time point) and were differentially expressed with a fold change greater than two (FC >2) between any of the six treatment groups at each time point. This bioinformatic analysis revealed 1263 differentially expressed genes on day 1 (Fig. 3*C*) and 3712 differentially expressed genes on day 6 (Fig. 3*D*) between the six treatment groups during MC3T3 differentiation. Interestingly, hierarchical clustering of differentially expressed genes reveals a grouping between low BMP2 concentration plus GSK126 with high concentration BMP2 alone or combination with GSK126. A clear hierarchical clustering separation occurs between these three highly osteogenic treatment groups when compared with the other three treatment groups with less osteogenic potential (vehicle, 10 ng/ml BMP2, and 5 $\mu$M GSK126). This global expression analysis demonstrates that BMP2 and GSK126 each induce different gene expression programs in differentiating MC3T3 cells. In addition, it appears that GSK126 enhances expression of BMP2-responsive genes; this compound may also indirectly inhibit genes suppressed by BMP2 during osteoblast differentiation.

### *Co-stimulation of bone-related genes by concurrent administration of BMP2 and GSK126*

To identify genes that are synergistically activated by BMP2 and GSK126, we selected for highly expressed genes (RPKM >0.3) that are induced by BMP2/GSK126 combination when compared with vehicle (FC >2 on day 1, FC >4 on day 6) and are also robustly up-regulated in the BMP2/GSK126 combination when compared with sole BMP2 and GSK126 treatments (FC >1.4 on day 1, FC >2 on day 6). These analyses reveal 23 co-activated genes with low BMP2 and GSK126 combination, whereas high BMP2 and GSK126 combination results in 18 co-stimulated genes on day 1 of osteogenic differentiation (Table S2 and Fig. 4*A*). Several of these genes (*e.g.* Dlx3, Ibsp, Wif1, Igfbp5, Hey1, and Nog) are implicated with skeletal formation. Nine of these genes are commonly up-regulated between low BMP2 plus GSK126 and high BMP2 plus GSK126 combinations. Both low and high concentrations of BMP2 in

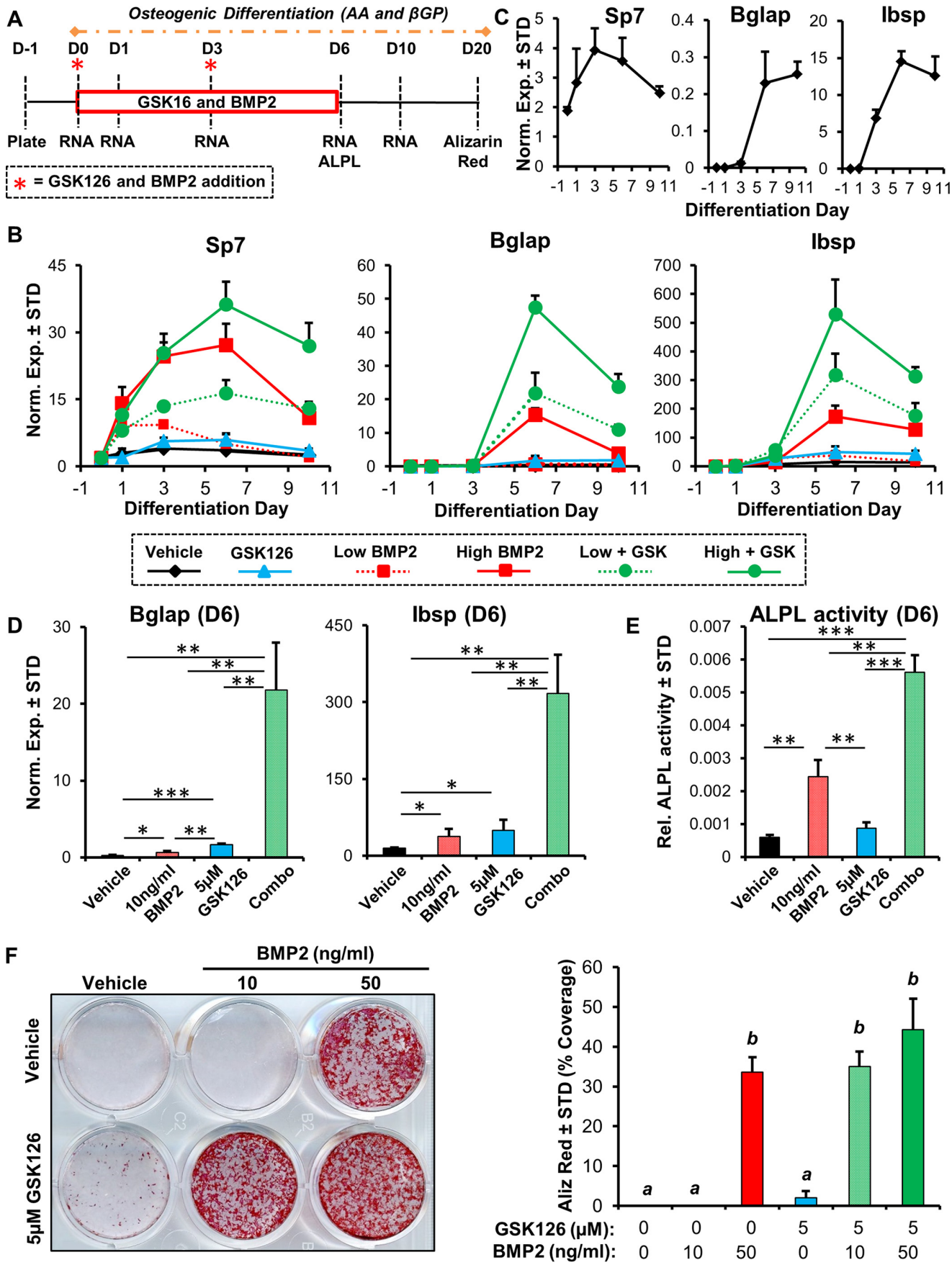
A
Osteogenic Differentiation (AA and βGP)
D-1
D0
D1
D3
D6
D10
D20
GSK16 and BMP2
Plate
RNA
RNA
RNA
RNA ALPL
RNA
Alizarin Red
* = GSK126 and BMP2 addition
C
Sp7
Bglap
Ibsp
Norm. Exp. ± STD
Differentiation Day
B
Sp7
Bglap
Ibsp
Norm. Exp. ± STD
Differentiation Day
Vehicle
GSK126
Low BMP2
High BMP2
Low + GSK
High + GSK
D
Bglap (D6)
Ibsp (D6)
Norm. Exp. ± STD
Vehicle
10ng/ml BMP2
5μM GSK126
Combo
E
ALPL activity (D6)
Rel. ALPL activity ± STD
F
BMP2 (ng/ml)
Vehicle
10
50
5μM GSK126
Aliz Red ± STD (% Coverage)
GSK126 (μM):
BMP2 (ng/ml):

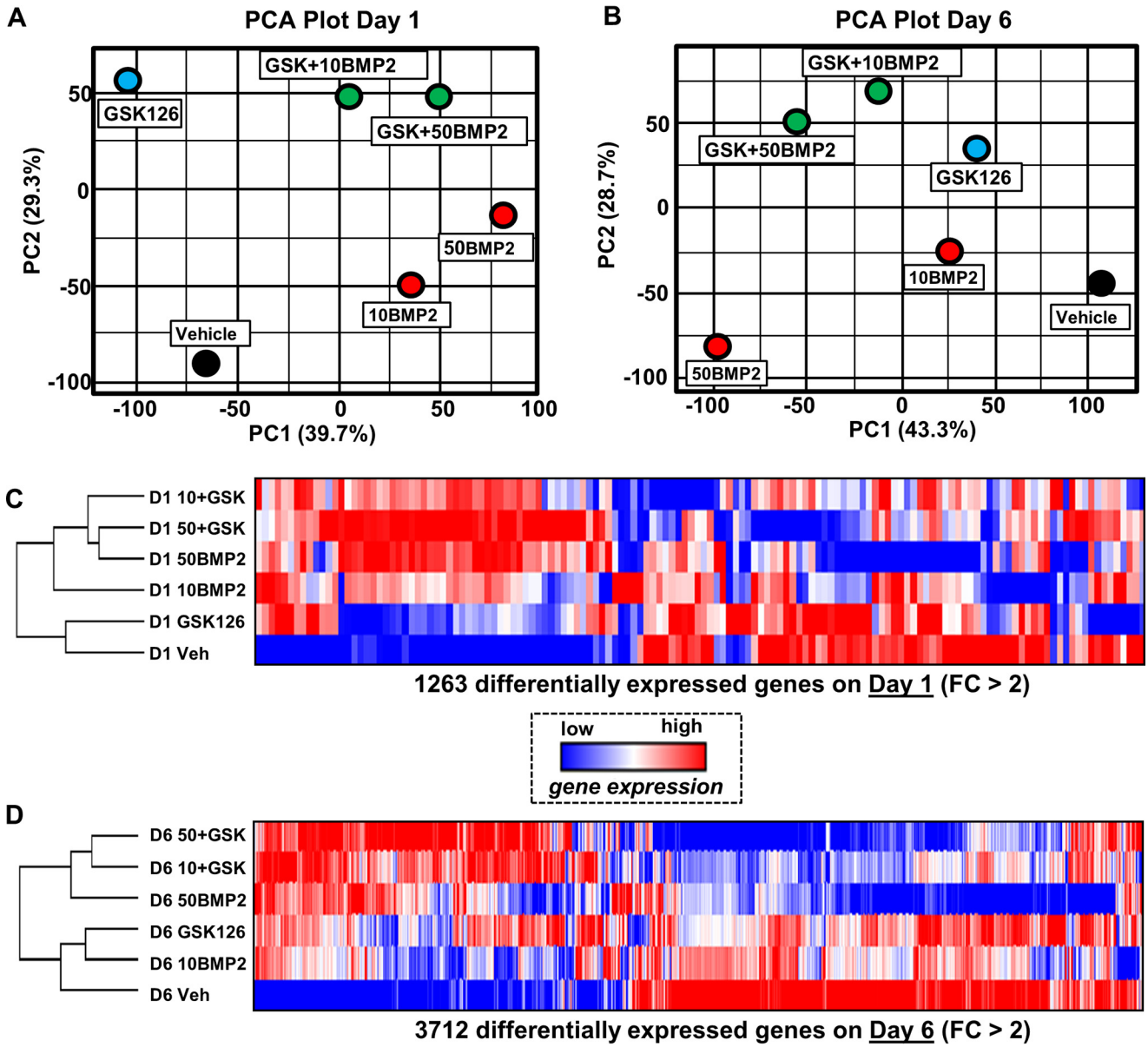


**Figure 3. Differential gene expression changes upon BMP2 and GSK126 treatment in MC3T3 cells.** RNA derived from differentiating MC3T3 cells treated with vehicle, GSK126, BMP2, and GSK126/BMP2 combination was assessed by mRNA-Seq analysis (see Fig. 2*A*, day 1 and day 6 samples). *A* and *B*, unbiased PCA on day 1 (*A*) and day 6 (*B*) of osteogenic differentiation (RPKM >0.3 in at least one group for each time point). The analysis included 11,974 (day 1) and 12,307 (day 6) genes. *C* and *D*, hierarchical clustering of differentially expressed genes on day 1 (*C*) and day 6 (*D*) of osteogenic differentiation. The analysis included genes that were detected by mRNA-Seq technology (average RPKM >0.1 across six samples at each time point) and were differentially expressed (FC >2 between any of the six treatment groups at each time point). The resulting hierarchical clustering is made up of 1263 (day 1) and 3712 (day 6) genes.

combination with GSK126 result in synergistic activation of 78 and 82 genes, respectively, of which 47 are common between the two combination groups on day 6 of osteoblast differentiation (Table S3 and Fig. 4*B*). Because of the significant overlap between the two drug combinations on day 6, additional bioinformatics analysis was performed on the commonly up-regulated genes ($n = 47$). DAVID 6.8 enrichment score analysis reveals several biological processes that are represented by these commonly up-regulated genes (Fig. 4*C*). Interestingly, 2 of 10 most highly enriched categories (*green bars*, biomineralization and ossification) are directly related to bone formation processes. To investigate potential protein–protein networks within the enriched gene set interactions, these 47 genes were assessed by STRING analysis (Fig. 4*D*). This analysis reveals a major protein–protein interaction network termed biomineral tissue development (*red circles*), which includes several well-characterized osteoblast/osteocyte-related genes (*e.g.* Ibsp, Phex, Bglap, Dmp1, and Spp1). In sum, these transcriptome

**Figure 2. BMP2 and GSK126 synergistically activate osteogenic differentiation of MC3T3 cells.** *A*, experimental protocol illustrating the treatment, differentiation, and analysis of MC3T3 cells. *B*, expression (RT-qPCR) of osteogenic markers (Sp7, Bglap, and Ibsp) at several time points ($n = 3$). *C*, expression (RT-qPCR) of osteogenic markers in the vehicle treated group ($n = 3$). *D*, expression (RT-qPCR) of Bglap and Ibsp on day 6 ($n = 3$). *E*, alkaline phosphatase activity assay on day 6 ($n = 3$). *F*, Alizarin Red staining (*left*) and quantification (*right*) on day 20 ($n = 3$). * = $p < 0.05$, ** = $p < 0.01$, *** = $p < 0.001$, *a versus b* = $p < 0.001$.

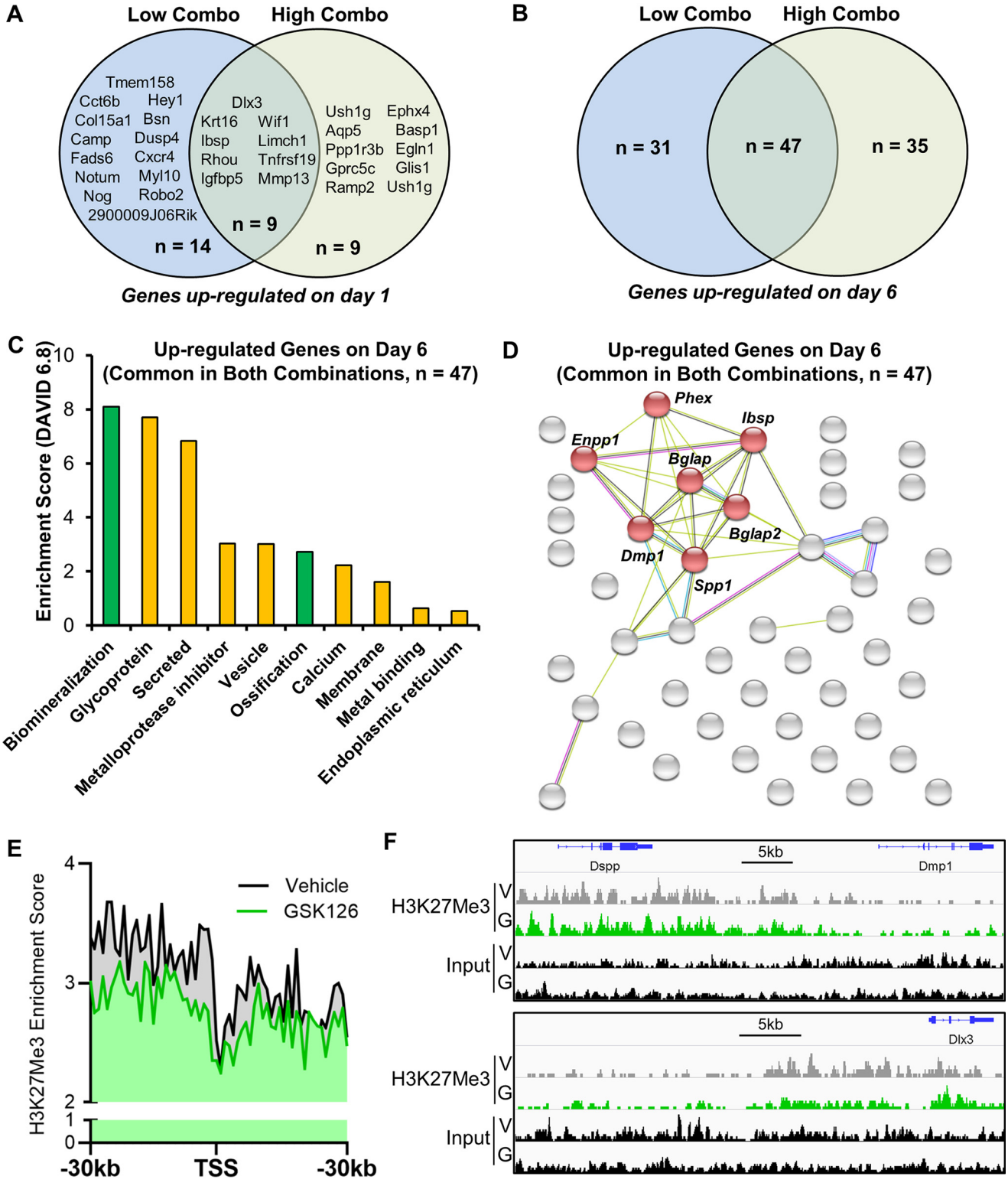


**Figure 4. Synergistic activation of osteogenic genes by dual administration of BMP2 and GSK126 in MC3T3 cells.** To identify genes that are synergistically activated by BMP2 and GSK126 administration, we selected for genes that are highly expressed (RPKM >0.3), are highly induced by BMP2/GSK126 combination when compared with vehicle treatment (FC >2 on day 1, FC >4 on day 6), and are enhanced by BMP2/GSK126 combination treatment when compared with individual BMP2 and GSK126 treatments (FC >1.4 on day 1, FC >2 on day 6). *A* and *B*, Venn diagram analysis showing genes that are synergistically activated when low (10 ng/ml) and high (50 ng/ml) BMP2 concentrations are combined with GSK126 (5 $\mu$M) on day 1 (*A*) and day 6 (*B*) of osteogenic differentiation. Gene list and expression profiles are shown in supporting materials (Tables S2 and S3). *C* and *D*, DAVID 6.8 enrichment score analysis (*C*) and STRING analysis (*D*) of synergistic genes commonly up-regulated in low BMP2 plus GSK126 and high BMP2 plus GSK126 treatment ($n = 47$) on day 6 of osteogenic differentiation. *E*, H3K27me3 enrichment analysis by ChIP-Seq of all genes that are up-regulated by low and high BMP2 plus GSK126 combination ($n = 113$, see *panel B*) in vehicle and 5 $\mu$M GSK126 treated (24 h) MC3T3 cells. *F*, ChIP-Seq track examples for Dmp1 and Dlx3 of input and H3K27me3 pull-downs in vehicle (*V*) and 5 $\mu$M GSK126 (*G*) -treated MC3T3 cells.

data demonstrate that the combination of BMP2 and GSK126 results in co-stimulatory up-regulation of genes that are involved in osteoblast-related processes.

Similar to co-stimulated genes, bioinformatic analysis reveals gene sets that are co-suppressed by the combination of BMP2 and GSK126 (Fig. S2 and Tables S2 and S3). Combination of either low BMP2 with GSK126 or high BMP2 with GSK126 results in the co-suppression of genes on day 1 (Fig. S2*A*) and day 6 (Fig. S2*B*) of osteogenic differentiation. However, there is no overlap on day 1 whereas only 19 genes overlap on day 6 when low and high BMP2 concentrations are combined with GSK126. Because of few overlapping genes ($n = 19$), DAVID 6.8 enrichment score analysis (Fig. S2*C*) and STRING analysis (Fig. S2*D*) on day 6 were performed on all co-suppressed genes ($n = 101$). Interestingly, enrichment score analysis reveals a robust suppression of genes related to cell division, including enriched categories such as cell cycle, chromosome, and microtubule. In support, protein–protein network interaction by STRING reveals an interaction network termed cell division (*blue circles*). Thus, these data demonstrate that, in addition to enhancing expression of osteogenic genes, the combination of BMP2 and GSK126 suppresses cell division in MC3T3 cells to generate a postproliferative state that supports differentiation.

To assess whether gene expression changes directly correlate with changes in H3K27me3 upon Ezh2 inhibition, ChIP-Seq analysis was performed on MC3T3 cells treated with vehicle and 5 $\mu$M GSK126 for 24 h. Our analysis is focused on up-regulated genes because the loss of H3K27me3 is associated with gene activation. Although our initial analysis demonstrated an overall reduction in H3K27me3, including in regulatory regions of key osteogenic loci (54), our current analyses focused on assessing H3K27me3 status of genes that are activated by dual administration of BMP2 and GSK126 (Fig. 4, *B–D*). These analyses reveal that 24-h treatment with 5 $\mu$M GSK126 reduces H3K27me3 levels at genomic regions of genes that are up-regulated by prolonged (6 days) GSK126 and BMP2 treatment during osteogenic differentiation (Fig. 4*E*). Because significant up-regulation of key osteogenic/osteocytic markers (*e.g.* Phex, Bglap, Dmp1, and Spp1) occurs by dual administration of BMP2 and GSK126, we assessed H3K27me3 levels at genomic regions of these bone-related genes. As illustrated by the Dmp1 locus (Fig. 4*F*), administration of GSK126 did not significantly alter H3K27me3 levels of mature osteoblast/osteocyte markers in MC3T3 cells. Because of the low number of loci that are activated by dual BMP2 and GSK126 treatment on day 1 (*i.e.* low BMP2 plus GSK126 and high BMP2 plus GSK126), it is not informative to perform general epigenomic profiling by averaging H3K27me3 marks across gene bodies. Yet, examination of loci-specific assessment reveals a significant reduction in H3K27me3 at genomic regions spanning the Dlx3 gene (Fig. 4*F*), a key osteogenic transcription factor that is up-regulated by the dual administration of GSK126 and BMP2 (Fig. 4*A*) and whose function is required for early stages of osteogenic differentiation (61). These results collectively indicate that activation of late osteoblast markers by dual administration of BMP2 and GSK126 may not be caused by changes in H3K27me3 at these loci, but rather may change Ezh2-mediated methylation events in the regulatory regions of osteogenic factors that are activated during earlier stages of osteoblast differentiation.

### *BMP2 and Ezh2 inhibition coordinately activate osteogenic lineage commitment in human bone marrow–derived MSCs (hBMSCs)*

To assess BMP2 and GSK126 interaction during osteogenic differentiation in an uncommitted nonimmortalized cell culture model, we utilized hBMSCs derived from commercially purchased bone marrow (62) (Fig. 5). As with pre-committed MC3T3 osteoblasts, hBMSCs were treated with BMP2 and GSK126 during the first 6 days of osteogenic differentiation (Fig. 5*A*). Similar to results with MC3T3 osteoblasts and human adipose–derived MSCs (hAMSCs) (44, 54), preventing the formation of new H3K27me3 marks by GSK126 reduces total H3K27me3 marks in a concentration-dependent manner in hBMSCs (Fig. 5*B*). However, unlike in MC3T3 and hAMSCs, inhibition of H3K27me3 formation by GSK126 does not completely eliminate H3K27me3 in hBMSCs. The latter finding suggests that attrition of H3K27me3 marks because of histone demethylation in hBMSCs proceeds slower than in MC3T3s and hAMSCs. Also, no appreciable effects of GSK126 are observed on EZH2, H3, and GAPDH protein levels, except for the highest concentration (10 $\mu$M). As anticipated, BMP2 treatment increases osteogenic gene expression in a concentration-dependent manner (Fig. 5*C*). For comparison, expression of the housekeeping gene AKT1 is not altered with BMP2 and GSK126 administration relative to GAPDH. We note that GSK126 treatment does not have a significant impact on the expression of bone-related genes during osteogenic differentiation of hBMSCs, presumably in part because H3K27me3 levels are less acutely down-regulated upon Ezh2 inhibition. Similar to MC3T3 osteoblasts, the addition of GSK126 increases the osteogenic effects of BMP2 treatment on gene expression in hBMSCs. Interestingly, co-stimulation is observed for GSK126 and high BMP2 concentrations on day 6 (*top graphs*), but the combination of GSK126 with a low BMP2 dose shows strongest co-stimulation on day 13 (*bottom graphs*). These findings demonstrate that BMP2 and GSK126 co-induce osteogenic lineage commitment of hBMSCs, complementing the co-stimulatory effects observed during osteoblast maturation of MC3T3 cells.

### *Co-administration of BMP2 and GSK126 results in more consistent bone healing*

Encouraged by our *in vitro* results, we performed initial feasibility studies to address whether BMP2 and GSK126 are able to co-stimulate bone formation *in vivo* in a critical-sized calvarial defect mouse model (Fig. 6) (63). The defect was created in the left parietal bone using a 2.5-mm dental trephine attached to a low-speed dental drill controlled by a manual foot pedal. The experiment was performed in adult (12 weeks old) C57BL/6J male mice, which were sacrificed and assessed 4 weeks after surgery (16 weeks of age). Vehicle, BMP2 (0.3 $\mu$g), GSK126 (5 $\mu$g), and the BMP2/GSK126 combination were administrated at the defect site at time of surgery. Mice also received (intraperitoneal injections) 50 mg/kg GSK126 or vehicle (DMSO) 1 day before surgery, on the day of surgery, and 3 consecutive days after surgery (54). X-ray analysis demon-

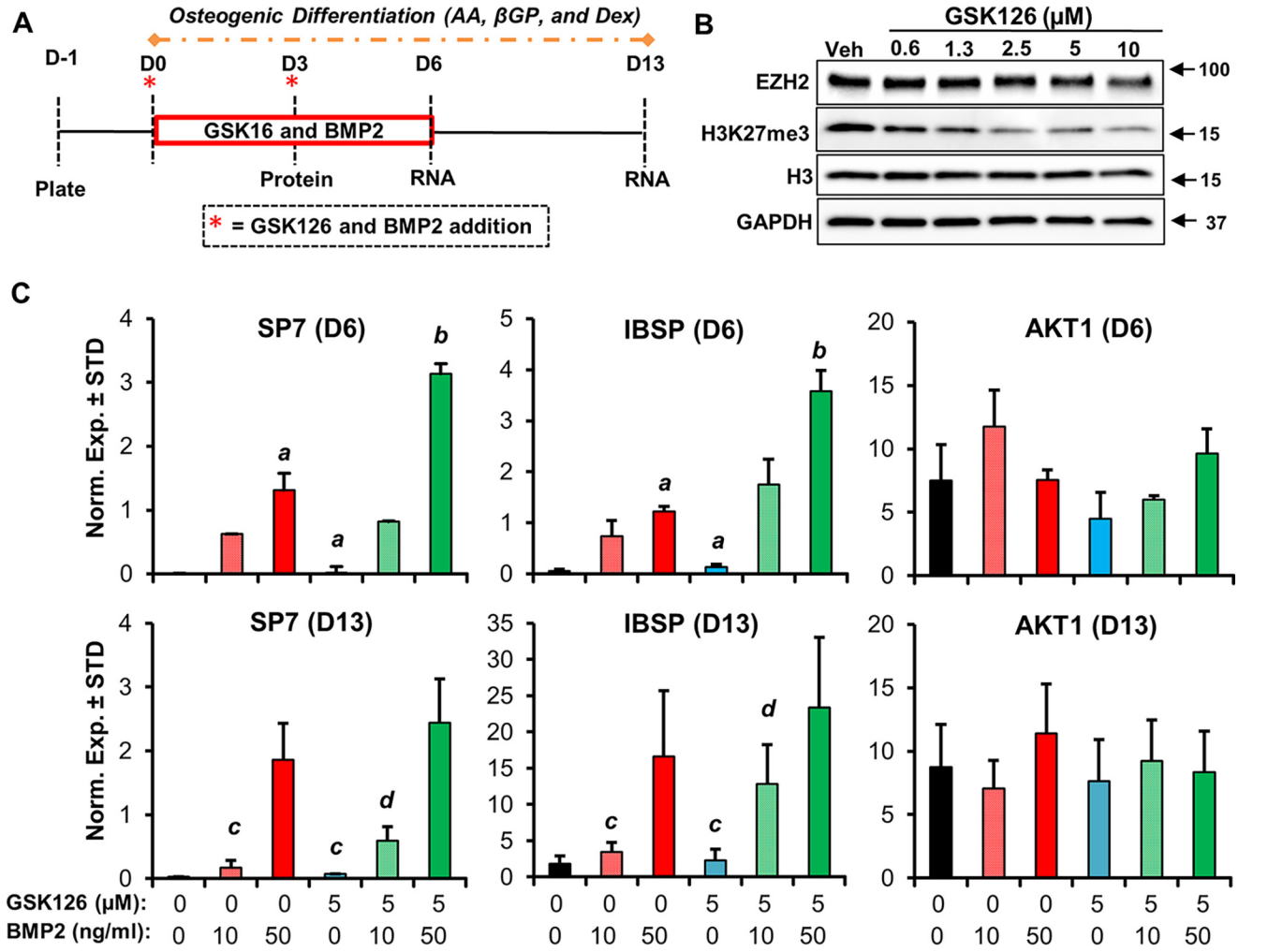


**Figure 5. GSK126 potentiates BMP2-induced expression of osteogenic genes in hBMSC.** *A*, experimental set-up for BMP2 and GSK126 treatment and osteogenic differentiation of hBMSCs. *B*, Western blot analysis of differentiating hBMSCs upon Ezh2 inhibition. Cells were treated with vehicle and varying GSK126 concentrations (0.6 to 10 μM). Protein was harvested and assessed on day 3 of osteogenic differentiation. *C*, RT-qPCR analysis of osteogenic markers (SP7 and IBSP) and AKT1 (housekeeping gene) during osteogenic commitment of hBMSCs ($n = 3$, *a versus b* = $p < 0.001$, *c versus d* = $p < 0.05$). Gene expression analysis was performed on days 6 and 13 of osteogenic differentiation.

strates minimal healing in the vehicle and GSK126-treated mice (Fig. 6*A* and Fig. S3). Although robust healing is observed in some BMP2-treated animals, several calvarial defects did not heal properly within this group. With one exception, mice exhibit robust calvarial healing with dual administration of BMP2 and GSK126. To quantify the healing process, micro-computed tomography (μCT) (Fig. 6, *B* and *D*) and histomorphometric (Fig. 6, *C* and *E*) analyses of the calvarial defects were performed. These studies revealed significant differences between various treatment groups when assessing for bone mineral density (BMD) and bone volume fraction (bone volume to total volume ratio (BV/TV)), including a robust difference between vehicle-treated mice and mice treated with the combination of both BMP2 and GSK126. Interestingly, μCT and histomorphometry reveal more consistent healing in the combination group when compared with the BMP2 group (note spread of *red versus green data points*).

As an additional quantification method, two orthopedic surgeons were tasked to blindly grade the healing process by scoring X-ray images of the calvarial defects (Fig. 7 and Fig. S3). We utilized a modified version of the method described by Spicer and colleagues (64). In this study (scale 0 to 5), a score of 0 indicates no bone formation whereas a score of 5 represents a completely healed defect (see "Experimental procedures" section for additional information) (Fig. 7*A*). In addition, the surgeons were also asked to rank order the calvaria defects ($n = 22$) from worst (score of 1) to best (score of 22) healed (Fig. 7*B*). Robust healing scores are evident in the BMP2 and combination groups (Fig. 7*A*). BMP2 is significantly different when compared with vehicle treatment when assessed by healing score and rank. Interestingly, the combination treatment of BMP2 and GSK126 is significantly different when compared with vehicle and GSK126 treatment as quantified by both methods. To assess the potential for observer bias, we examined the healing score and rank between the two surgeons. The interobserver correlation was excellent between both orthopedic surgeons, with a Spearman's Rho (ρ) of 0.93 for healing grade and 0.91 for overall rank in terms of healing (Fig. 7*C*). Taken together, the μCT and histomorphometry results, as well as the surgeon-defined healing score and rank indicate that BMP2 and the combination of both BMP2 and GSK126 mediate robust bone healing. However, the healing scores revealed a

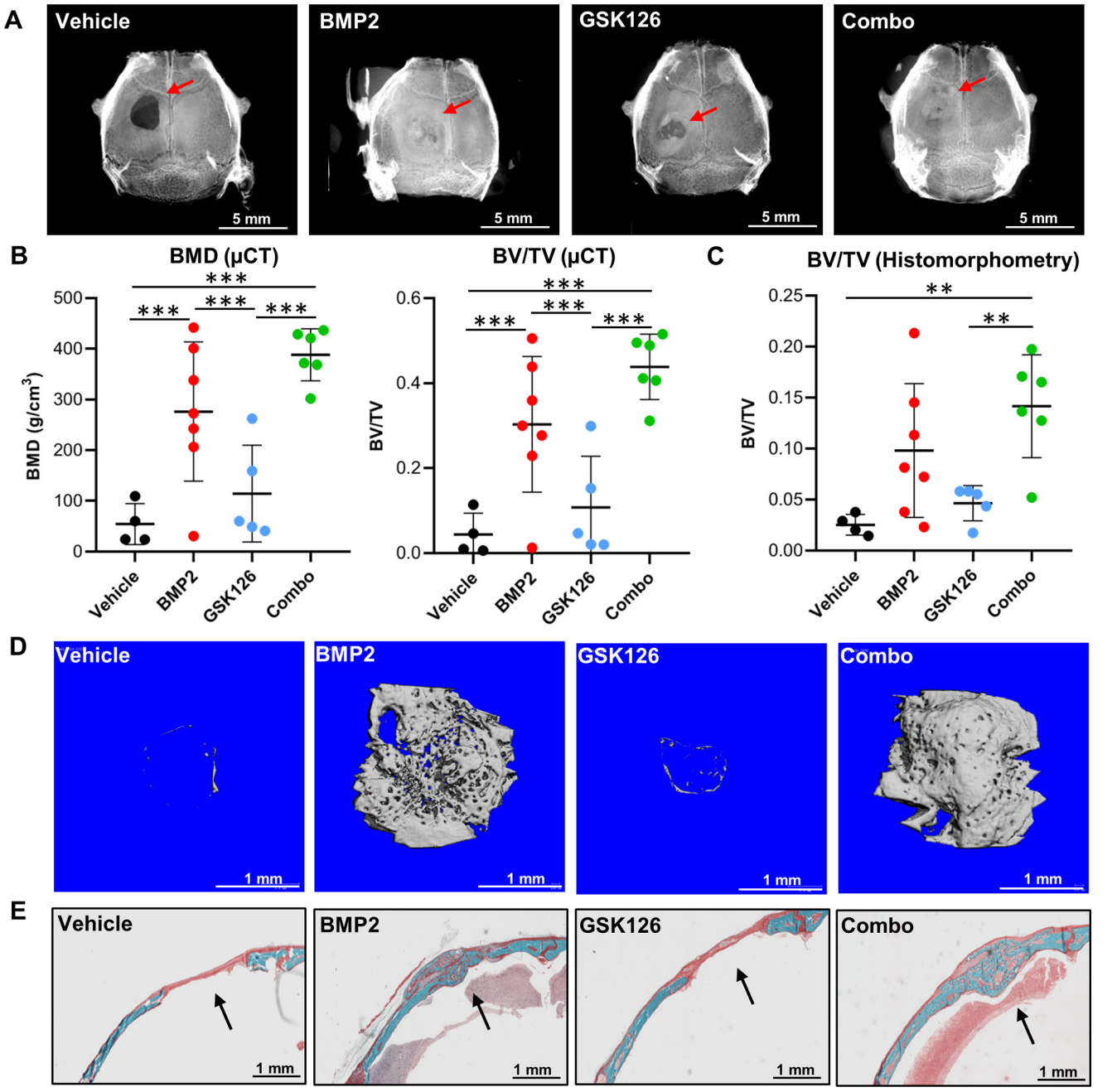


**Figure 6. BMP2 and GSK126 combination results in more consistent bone healing.** Critical-sized calvarial defect model (left parietal bone) was created and treated (vehicle, BMP2, GSK126, and combination of BMP2 and GSK126) as described in "Experimental procedures." Relevant tissues (skulls/calvaria) were harvested and processed 4 weeks (28 days) after the surgery. *A*, representative x-rays of four treatment groups. *B* and *C*, X-rays of all defects are shown in Fig. S3. µCT (*B*) and histomorphometric (*C*) quantification of the calvarial defect model ($n = 4$ to 7, mean ± STD, ** = $p < 0.01$, *** = $p < 0.001$). Each point on the graph represents an individual mouse. Defect margins were identified and native bone was excluded from the quantification. *D* and *E*, examples of µCT scans (*D*) and histologic coronal staining (*E*) of calvarial defects for each treatment group.

more consistent healing in the combination group when compared with BMP2 alone.

To address potential differences in healing consistencies between BMP2 and BMP2/GSK126 combination, additional statistical analysis was performed to assess for variance. In regard to the distribution of the data points, the point estimate of the variance for BMP2 *versus* the combination group favors the combination group as more consistent (lower estimated variance) in every comparison made (BMD, BV/TV (µCT), BV/TV (histomorphometry), healing score, and healing rank (see Figs. 6 and 7). The statistical odds that five of five comparisons of variance estimates favor the same group (BMP2 plus GSK126) are unlikely to be driven by chance alone ($p = 0.01$). The distribution of data for BMD, as presented in Fig. 6*B*, reveals a variance of 18,861 for the BMP2 group and 2633 for the combination group (7-fold less variance, $p = 0.047$). Similarly, the variance of BMP2 BV/TV via µCT is 0.026, as compared with 0.006 for the combination group, representing over 4-fold less variance for the combination group ($p = 0.13$). For histomorphometric evaluation, the variance of BMP2 scoring is

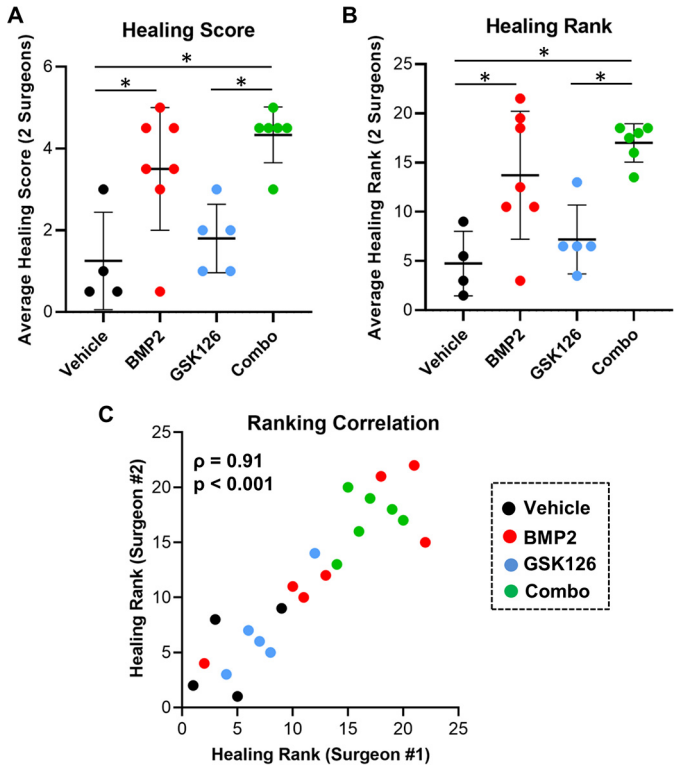


**Figure 7. Healing consistency within the BMP2 and GSK126 group is supported by orthopedic surgeon assessment.** *A* and *B*, defect X-rays were scored blindly based on healing score (0, no healing to 5, completely closed) (*A*) and healing rank (1, worst healed to 22, best healed) (*B*) by two orthopedic surgeons (* = $p < 0.05$). The scores are averages of the scores and ranks given by the two orthopedic surgeons. Detailed methodology is described in the "Experimental procedures" section. *C*, correlation graph confirming consistent defect ranking by the two orthopedic surgeons.

2.25 compared with 0.5 for the combination group ($p = 0.11$). Finally, when assessing healing rank (see Fig. 7*B*), the variance for BMP2 is 42.3, as compared with the combination group variation of 3.8, or 10-fold less ($p = 0.02$). In sum, our statistical assessment for variance indicates that the combination group yields more consistent healing when compared with BMP2 treatment alone.

Taken together, our feasibility studies to examine the effects of co-treating a bone defect with both BMP2 and GSK126 are encouraging. These initial *in vivo* studies revealed that both drugs are compatible: At a minimum, the results show that GSK126 does not antagonize the osteogenic effects of BMP2 and, in a more optimistic interpretation, may reduce individual variation in healing outcomes (*e.g.* perhaps by accelerating the bone repair process).

## Discussion

We and others have demonstrated that Ezh2 is required for skeletal development and recognized the concept that inhibition of this epigenetic enzyme can enhance bone formation *in vitro* and *in vivo* (42–56). The established evidence suggests that the pro-osteogenic effects of Ezh2 inhibition arise from de-repression of osteogenic genes (*e.g.* Sp7) as well as stimulation of osteogenic pathways through up-regulation of ligands (e.g.,Wnt10b), receptors (Pth1r), and posttranslation modification (*e.g.* Smad1/5 phosphorylation) (39, 54). Based on this evidence, we hypothesized that inhibition of Ezh2 may be combined with established bone anabolic therapeutics to stimulate osteogenesis and bone formation. Combining Ezh2 inhibition with BMP2 treatment is especially attractive as lowering concentration of this ligand could enhance its therapeutic potential, lower its side effects, and may reduce costs associated with its use (2, 33, 34). Consequently, this study assessed the effects of combining BMP2 and GSK126 (Ezh2 inhibitor) on osteogenesis *in vitro* and bone healing *in vivo*.

Our current studies confirm the previously established pro-osteogenic effects of Ezh2 inhibition (GSK126) in MC3T3 cells (54). Although Ezh2 inhibition has also been shown to stimulate osteogenic commitment of hAMSCs (44), we did not observe an enhancement in the expression of osteogenic genes in hBMSCs treated with GSK126. These divergent effects could be attributed to the varying levels and stability of H3K27me3 levels upon Ezh2 inhibition. Consistent with this reasoning, although H3K27me3 is completely eliminated by 2 $\mu$M GSK126 in hAMSCs (44), a significant amount of H3K27me3 is observed when hBMSCs are treated with 10 $\mu$M GSK126 (present study). The different sensitivities to Ezh2 inhibition may be because of varying pharmacodynamics and pharmacokinetics (*e.g.* cellular import and export of GSK126, and drug metabolism), as well as molecular differences in Ezh2 regulation (*e.g.* Ezh2 protein turnover) in different cell types. It is also possible that different expression patterns or activities of the other H3K27 methyltransferase (Ezh1) and opposing H3K27 demethylases (Jhdm1d, Kdm6a, and Kdm6b) may contribute to varying cellular responses to Ezh2 inhibition (*i.e.* GSK126) (38–40, 65).

The pro-osteogenic effects of BMP2 were established about three decades ago (3, 4, 66–68). As anticipated, BMP2 stimulates osteogenic differentiation of MC3T3s and hBMSCs in a concentration-dependent manner. Previous studies have suggested that modifying the DNA and histone protein epigenomes may enhance BMP2-induced osteogenesis (50, 69–72). We show here that combination of BMP2 and Ezh2 inhibition (GSK126) results in strong co-stimulatory enhancement of MC3T3 and hBMSC differentiation. Importantly, we establish that dual GSK126 and BMP2 treatment results in enhanced expression of key osteoblastic/osteocytic genes (*e.g.* Dmp1) that is accompanied by a reduction in genes related to cell division. These findings are in line with studies showing that BMP2 enhances osteogenesis while also suppressing cell proliferation in differentiating cells (73, 74). Similarly, inactivation of Ezh2 is associated with enhanced osteogenic differentiation and cell cycle alterations (44, 47, 54). Interestingly, although GSK126 reduces overall H3K27me3 at genomic regions of genes activated by the combination of BMP2 and GSK126, our analysis did not reveal significant alterations in histone methylation of late osteogenic markers such as Dmp1, suggesting that activation of more proximal events linked to key osteogenic transcription factors (*e.g.* reduction of H3K27me3 at the Dlx3 locus) may support the pronounced co-stimulated activation of late phenotypic markers of osteogenic differentiation.

One key question is how synergism between GSK126 and BMP2 signaling during osteoblast differentiation is achieved. This question requires consideration of temporal and causative perspectives at both molecular and cellular levels. Pharmaco-

logical doses of GSK126 (0.2–2.0 $\mu$M) quantitatively reduce deposition of H3K27me3 marks in MSCs and osteoblasts within 6 h (44, 54). Within several days, the loss of gene-suppressive H3K27me3 marks results in the activation of quiescence-related genes to stop proliferation and promotes osteogenic differentiation by stimulation of PTH, WNT, and BMP signaling pathways (44, 47, 54). Yet, mature osteoblast-specific genes (*e.g.* Bglap/osteocalcin) are not maximally expressed until at least 10 days after initiation of osteoblast differentiation (54). Hence, GSK126-dependent demethylation is a mechanistic event that occurs very proximal to osteoblast maturation.

Exogenous administration of BMP2 rapidly induces the serine/threonine kinase activity of BMP receptors (*e.g.* Bmpr1a, Bmpr2) that phosphorylate Smad1-Smad5; phospho-Smad1/5 then interacts with Runx2 and induces expression of the Bglap/osteocalcin which is directly controlled by at least three Runx2-binding sites (1, 75–78). Thus, BMP2 signaling directly connects the bone morphogenic activity of BMP2 to the transcriptional activity of a bone-specific master regulator via protein phosphorylation. Therefore, biological synergy between Ezh2 inhibition and BMP2 is not mediated at the molecular level but must be understood at the level of cellular pathways.

Although BMP receptor–dependent protein kinase activity at the cell surface cannot alter the Ezh2-dependent methylation of H3K27me3 in the nucleus, our previous data have shown that inhibition of H3K27me3 enhances the expression of genes that activate the endogenous BMP2–BMP receptor–Smad1/5 axis (54). Consistent with this model, we find that Ezh2 inhibition by GSK126 in MC3T3 osteoblasts decreases H3K27me3 at the Dlx3 locus and increases expression of Dlx3; Dlx3 is closely related to Dlx5 and both represent osteogenic and BMP2-responsive homeodomain transcription factors. Because Dlx3/5 proteins act initially upstream of RUNX2 (11, 12), and because Runx2 is upstream of the BMP2 responsive Sp7/Osterix protein (11, 79), it is apparent that GSK126 accelerates early stages of osteoblast differentiation by direct effects on Dlx3 and indirectly on the molecular interplay between Dlx3, Runx2, and Sp7.

BMP2 signaling during osteoblast differentiation is thought to activate several positive and negative feedback loops to ensure orderly progression of osteoblast differentiation. For example, activation of endogenous production of BMP2 proteins by osteoblasts is expected to ensure sustained paracrine signaling of this potent osteogenic morphogen (70, 80, 81). This study shows that GSK126 reduces the deposition of epigenetic marks that normally suppress expression of BMP2-responsive osteogenic genes such as Dlx3. Hence, GSK126 preconditions and facilitates the BMP2 response by reducing epigenetic barriers in chromatin. This mechanism is known as epigenetic priming and has been described previously in the cancer field to clarify the enhanced efficacy of anticancer drugs in the presence of epigenetic inhibitors (37, 82, 83). The general significance of our findings is that it extends the concept of epigenetic priming as a cancer therapy into a viable strategy for promotion of osteoblast differentiation in bone-regenerative medicine.

As part of ongoing studies aimed at developing strategies to promote bone formation and healing, our groups recently developed a mouse calvarial critical-sized defect model (63). We applied this model in our studies as an illustration of the translational potential of our work. As anticipated, local administration of BMP2 resulted in robust healing 4 weeks after defect formation. Our current studies confirm the healing potential of local administration of BMP2, but administration of GSK126 (local plus global) did not quantitatively improve the healing process. The *in vivo* results were less impressive than our *in vitro* findings, because combination of BMP2 and GSK126 did not result in statistically significant differences in healing compared with BMP2 alone. However, GSK126 certainly did not antagonize the osteogenic effects of BMP2 and co-treatment appeared to be trending toward modestly improved healing. The encouraging finding of these studies is that the combination regimen resulted in more consistent healing compared with BMP2 treatment alone, as measured by analytical techniques ($\mu$CT and histomorphometry) and subjective measurements by orthopedic surgeons (healing score and rank).

Combination treatment of GSK126 and BMP2 yields more consistent calvarial bone healing compared with BMP2 alone based on statistical assessment of variance. Our bone healing scores were based on end point analysis, which shows significant variation in the extent of bone healing. The latter is attributable to individual differences in the rate of bone formation in mice. Although GSK126 cannot quantitatively increase bone healing beyond completion (*i.e.* 100%), it can temporally accelerate healing, which is expected to decrease individual variation in end point healing scores. Hence, the observed reduction in variance for the combination of GSK126 and BMP2 is not inconsistent with improved healing relative to BMP2 alone.

While *in vitro* experimentation allowed for titration of BMP2 and GSK126 to establish a synergistic interaction, our *in vivo* studies were limited to previously established delivery methods and dosing regimens for these pro-osteogenic agents. One of the limitations of our study is the timing of BMP2 and GSK126 delivery, which may have reduced overall efficacy of the co-treatment. BMP2 was delivered locally whereas GSK126 was delivered locally and systemically (initial 5 days). Fine tuning GSK126 administration may result in more pronounced and increasingly titratable combinatory effects. Loss of Ezh2 activity has been shown to induce cell cycle alteration in primary mesenchymal stem cells, and balancing the desired effects (*i.e.* enhanced osteogenesis) (44, 54) with potential side effects (*i.e.* cell cycle arrest) (47) may be required to best harness the beneficial effects of Ezh2 inhibition. Future studies on the optimization of dosing for both BMP2 and Ezh2 may consider several routes of deliveries and assess whether it is realistic to have both treatments be given at the same times, which would ultimately be preferable from a surgical standpoint. Another limitation of our *in vivo* study is the administration of 300 ng BMP2, a dose which was shown by our group to stimulate calvarial defect healing in mice (63). This BMP2 dosing regimen is similar to other calvarial defect healing mouse studies (84–86). Yet, this dose was optimized to support efficient bone healing with BMP2 and hence would not be the most effective method for examining the efficacy of BMP2 in the presence of GSK126, which ideally would be performed with suboptimal doses. Of interest, while our study was in progress, Reyes *et al.* (86) dem-

onstrated that BMP2-induced healing can be enhanced by MMP10 co-administration at 4 weeks but not at 8 weeks post surgery. Thus, future studies on the impact of Ezh2 inhibition on BMP2-mediated calvarial healing should examine earlier stages of the bone healing process and consider lower doses of BMP2.

The key finding of this study is that co-incubation of BMP2 with an epigenetic drug (the Ezh2 inhibitor GSK126) primes osteoblast differentiation in culture. Our present study demonstrates that short-term application of GSK126 is sufficient to greatly enhance osteogenic effects of BMP2 *in vitro* in MC3T3s and hBMSCs. Thus, it may be possible to condition or program MSCs with BMP2 and epigenetic drugs such as GSK126 *ex vivo* before implantation into bone defects to enhance the desired bone anabolic effects. This approach may be more appropriate in the case of Ezh2 inhibitors as the osteogenic effects can be maximized and the undesired effects virtually eliminated as the recipient (study animal or human) would not come in contact with drug but rather epigenetically modified cells. Indeed, studies have shown that engineered hAMSCs overexpressing BMP2 and miR-148b (miRs/microRNAs are a form of epigenetic regulation) result in robust calvarial defect healing in immunocompromised mice (87, 88). Mechanistically, it was concluded that miR-148b enhanced and prolonged BMP2 expression to stimulate osteogenesis both *in vitro* and *in vivo*.

Recent studies on Ezh2 and its inhibitors have suggested that it may be possible to manipulate H3K27 methylation to stimulate osteogenesis and bone formation. Although previous evidence demonstrated bone anabolic and osteoprotective effects of Ezh2 inhibitors in mouse models of osteoporosis (54–56), our current evidence suggests that Ezh2 inhibition is not sufficient to enhance the bone healing process *in vivo*. However, our studies suggest that Ezh2 inhibition may provide the basis for new strategies for epigenetic priming to enhance the osteogenic effects of BMP2 *in vitro* and perhaps *in vivo*.

## Experimental procedures

### *MC3T3 cell culture*

MC3T3 sc4 murine calvarial osteoblasts (89) were purchased from American Type Culture Collection and maintained in $\alpha$-minimal essential medium without ascorbic acid (Gibco) containing 10% fetal bovine serum (Atlanta Biologicals), 100 units/ml penicillin, and 100 $\mu$g/ml streptomycin (Gibco).

### *hBMSC cell culture*

hBMSCs were isolated from bone marrow mononuclear cells purchased from Lonza (cat. no. 2 M-125C) by plastic adherence. Briefly, frozen bone marrow mononuclear cells were thawed in maintenance media comprised of advanced minimum essential medium (Gibco) containing 10% fetal bovine serum, 2 mM L-glutamine (Gibco), 100 units/ml penicillin, and 100 $\mu$g/ml streptomycin. Cell suspensions were centrifuged at 200 $\times$ *g* for 15 min for three cycles; cell pellets were re-suspended in maintenance media and at 30,000 cells/cm$^2$. Cells were allowed to adhere for 7 days following which nonadherent cells in the media were removed by aspiration. Fresh medium was added and replaced every 3–4 days. Adherent cells were allowed to form colonies and expand for 3–5 weeks after which colonies were harvested and re-plated at 5000 cells/cm$^2$. Cells from passage 4–6 were used for all *in vitro* and *in vivo* experiments.

### *Osteogenic differentiation*

For osteogenic differentiation, MC3T3s and hBMSCs were seeded in respective maintenance medium at a density of 10,000 cells/cm$^2$. Next day, osteogenic medium supplemented with vehicle, GSK126 (Xcess Biociences Inc.), recombinant human/mouse/rat BMP2 (R&D Systems; 355-BM), and combination of GSK126/BMP2 was added to the cells. Osteogenic medium for MC3T3 cells consisted of 50 $\mu$g/ml ascorbic acid (Sigma) and 4 mM $\beta$-glycerol phosphate (Sigma). Osteogenic medium for hBMSCs contained 50 $\mu$g/ml ascorbic acid, 8 mM $\beta$-glycerol phosphate, and $10^{-8}$ M dexamethasone (Sigma). Three days later, old medium was replaced with a fresh batch of osteogenic medium supplemented with vehicle, GSK126, BMP2, and combination of GSK126/BMP2. On day 6 of differentiation, fresh osteogenic medium without supplements was added and replenished every 2 to 3 days.

### *Real-time reverse transcriptase PCR (RT-qPCR)*

Total RNA was isolated using the Direct-zol™ RNA kit (Zymo Research) and quantified using the NanoDrop 2000 spectrophotometer (Thermo Fischer Scientific). RNA was then reverse transcribed into cDNA by the SuperScript III First-Strand Synthesis System (Invitrogen). Transcript levels were then measured using the $2^{\Delta\Delta Ct}$ method and normalized GAPDH (set at 100), a housekeeping gene. Gene-specific primers are shown in Table S4.

### *Western blotting*

Cell lysis and Western blotting were performed as described previously (44, 47, 48, 54). Proteins were visualized using the ECL Prime detection kit. Primary antibodies used were actin (1:10,000; sc-1616; Santa Cruz Biotechnology), H3 (1:10,000; 05-928; Millipore), and H3K27me3 (1:5000; 17-622; Millipore).

### *Alkaline phosphatase activity assay*

On day 6 of osteogenic differentiation, media were removed and cells were washed one time with PBS. Tris-EDTA buffer (0.1×) was then added to the wells to completely cover the cells. The plate was then stored at −80 °C for at least 2 h and then thawed back to room temperature. 500 $\mu$l of *para*-nitrophenylphosphate solution (2.5 mg 4-nitrophenylphosphate disodium salt hexahydrate (Sigma) per 1 ml of buffer (0.1 M diethanolamine, 150 mM NaCl, 2 mM $MgCl_2$)) was added to each well. The plate was incubated for 30 min (time may vary) at room temperature before measuring absorbance at 405 nm using the SpectraMAX Plus spectrophotometer. Values were fit to a standard curve prepared using reconstituted alkaline phosphatase enzyme (Roche) to determine relative enzymatic activity.

### *Alizarin Red staining*

Cells were fixed in 10% neutral buffered formalin and stained with 2% Alizarin Red (Sigma) to visualize calcium deposition.

Absorption of Alizarin Red stain was quantified with ImageJ software (90).

### Animal welfare

Animal studies were conducted according to guidelines provided by the National Institutes of Health and the Institute of Laboratory Animal Resources, National Research Council. The Mayo Clinic Institutional Animal Care and Use Committee approved all animal studies. Animals were housed in an accredited facility under a 12-hour light/dark cycle and provided water and food (PicoLab Rodent Diet 20, LabDiet) *ad libitum*.

### Calvarial defect healing model

Assessment of calvarial healing was performed in 12-week-old male C57BL/6J mice purchased from The Jackson Laboratories. This critical-sized calvarial defect model was recently described in great detail (63). Briefly, a 2.5-mm dental trephine attached to a low-speed (~1500 rotations per minute) dental drill controlled by a manual foot pedal was used to generate a critical-sized defect in the left parietal bone. A fibrin clot was prepared using the TISSEEL kit (Baxter) for drug delivery. Vehicle, BMP2 (0.3 $\mu$g), GSK126 (5 $\mu$g), and BMP2/GSK126 combination was prepared at a final volume of 6 $\mu$l, mixed with 6 $\mu$l of thrombin solution, and then combined with 6 $\mu$l of sealer protein to form the fibrin clot. The prepared biomaterial was placed into the defect site. In addition to local administration, 50 mg/kg GSK126 and vehicle (DMSO) were also administered by intraperitoneal injections (20% Captisol adjusted to pH 4–4.5 with 1 Normality (N) acetic acid) 1 day before surgery, on the day of surgery, and 3 days after surgery as described (54). Mice were euthanized 4 weeks after surgery. Skulls were harvested, fixed in 10% neutral buffered formalin for 48 h, and stored in 70% ethanol. Skulls were assessed by $\mu$CT and histomorphometry.

### $\mu$CT analysis

Calvarial defects were scanned using a Scanco vivaCT40 system (Scanco) at 70 kV, 114 $\mu$A with an integration time of 221 ms for a 10.5 isometric voxel size. 3D renderings were created using Microview (Parallax). Regions of interest were hand traced to isolate healing bone from native calvarial bone. A software-specific threshold of 220 (which corresponds to 2500 HU) was used to define mineralized tissue. Standard morphometric parameters were measured using Scanco software.

### X-ray analysis

After $\mu$CT analysis, skulls were dissected to remove all bone structures that are located underneath calvarial bones. The removal of all these bones allowed for a clear visualization of the defects by X-ray analysis. X-rays of calvarial defects were taken utilizing the same settings (Faxitron, LX60).

### Histomorphometry

Following $\mu$CT and X-ray assessment, histomorphometry was performed as described previously (47, 54, 63). Briefly, skulls were embedded in methyl methacrylate resin and sectioned using a rotary retracting microtome to generate 5-$\mu$m thick coronal sections. The resulting sections (widest point of the defect) were then stained by Gomori's trichrome (91). Quantitative histomorphometry was performed utilizing Bioquant Osteo Image Analysis Software (Bioquant) to establish the percentage of BV/TV. A box of 3.45 $mm^2$ (2.3 mm by 1.5 mm) was used for data quantification.

### Healing score and rank analysis

Healing score was assessed as described by Spicer *et al*. (64) with a modification. Spicer and colleagues utilized a scale that is based on a score between 0 and 4 (0 = no bone formation within defect, 1 = few bony spicules dispersed through defect, 2 = bony bridging only at defect borders, 3 = bony bridging over partial length of defect, and 4 = bony bridging entire span of defect at longest point). We added an additional point to the scale (5 = completely closed defect) to account for completely healed calvarial defects as measured by X-ray analysis. In addition to the scoring, we also rank ordered the healing calvarial defects (0–22, 0 = worst healed, 22 = best healed). The scoring and ranking was blindly performed by two orthopedic surgeons. Their scores were then averaged and graphed.

### High throughput RNA sequencing and bioinformatic analysis

RNA from differentiating MC3T3 cells treated with vehicle, GSK126, BMP2, and GSK126/BMP2 combination (Fig. 2*A*) were assessed by RNA-Seq analysis as reported previously (44, 47, 48, 54, 92, 93). For each condition and time point, equal amounts of RNA from three biological replicates were pooled and then subjected to RNA-Seq analysis. Gene expression is expressed in reads/kilobase pair/million mapped reads (RPKM). RNA-Seq data were deposited in the Gene Expression Omnibus of the National Center for Biotechnology Information (GSE135984). Venn diagrams were generated using Venny 2.1 online tool (BioinfoGP). PCA was performed using ClustVis online tool (60). Functional annotation clustering of differentially expressed genes was performed using DAVID Bioinformatics Resources 6.8 database (DAVID 6.8) (94, 95). Hierarchical clustering was performed using Morpheus matrix visualization and analysis software after a Log2 adjustment was made for each gene row (Broad Institute). Protein–protein interaction networks were generated using STRING Database version 10.5 (96).

### ChIP-Seq analysis

H3K27Me3 status at BMP2 and GSK126 activated genes was assessed using publically available ChIP-sequencing data sets (GSE83506) (54, 98). In brief, ChIP-Seq assay was performed 24 h after administration of vehicle (DMSO) or 5 $\mu$M GSK126 to MC3T3 cells cultured in osteogenic media (50 $\mu$g/ml ascorbic acid and 4 mM beta glycerol phosphate) (54). Read coverage over the mm10 genome was determined using the deepTools2 bamCoverage package (97). H3K27Me3 intensity was then assessed at specific genomic regions for the 113 genes identified as up-regulated at day 6 after BMP2 and GSK126 treatment using the deepTools2 computeMatrix package (97). Bin size was set to 1000 bases and coverage was assessed 30 kb upstream of the TSS and 30 kb downstream of the TES. Resulting values were visualized using GraphPad Prism 8.2.0. (San Diego, CA USA) (RRID:SCR_002798).

### *Statistics*

For *in vitro* studies, data are shown as mean ± S.D. and statistical analysis was performed with unpaired Student's *t* test or ANOVA. When the overall ANOVA F-test was significant, subsequent pairwise comparisons were performed using two-way ANOVA. For *in vivo* studies, the data are summarized using mean and S.D. unless otherwise noted. Each calvarial defect (mouse) is represented by a data point within the figures. The *in vivo* study outcomes were compared between the four experimental groups (vehicle, BMP2, GSK126, GSK126 + BMP2) using one-factor ANOVA. Separate analyses were performed for each outcome. When the overall ANOVA F-test was significant, pairwise comparisons were performed between the experimental groups using the Ryan-Einot-Gabriel-Welsch multiple comparisons test to maintain the overall type-I error rate at $\alpha = 0.05$. Significance is noted in the figures, when applicable (*, $p < 0.05$; **, $p < 0.01$; and ***, $p < 0.001$).

## Data availability

RNA-Seq (GSE135984) data have been deposited in the Gene Expression Omnibus of the National Center for Biotechnology Information. All other data are contained within the manuscript.

*Acknowledgments*—We thank current and past members of our laboratories, including Scott Riester, Farzaneh Khani, Leila Bagheri, Sofia Jerez, Margarita Carrasco Jeldres, Eric Lewallen, and Emily Camilleri for stimulating discussions. We acknowledge the support of Asha Nair from the Bioinformatics Core, Dirk Larson from Biomedical Statistics and Informatics, Medical Genome Facility, as well as Biomaterials Characterization and Quantitative Histomorphometry Core Facility. We thank William Shaughnessy for providing administrative supervision and guidance to Daniela Galeano-Garces.

*Author contributions*—A. D., R. M. S., and A. J. v. W. conceptualization; A. D., R. M. S., C. R. P., M. O. M., O. P., and R. T. data curation; A. D., R. M. S., C. R.P., P. K., M. K., A. N. L., and J. J. W. formal analysis; A. D., P. K., M. K., A. N. L., J. J. W., and A. J. v. W. supervision; A. D., R. M. S., C. R. P., C. G.-G., M. O. M., D. G.-G., P. Z., M. L. G., M. H., R. T., and A. J. v. W. investigation; A. D., R. M. S., C. R. P., C. G.-G., D. G.-G., P. Z., M. L. G., O. P., D. L. B., and S. M. C. methodology; A. D. writing-original draft; A. D. and A. J. v. W. project administration; A. D., P. K., A. N. L., J. J. W., S. M. C., and A. J. v. W. writing-review and editing; M. H. software.

*Funding and additional information*—This work was supported by National Institutes of Health Grant R01 AR049069 (A. J. v. W.) and a Career Development Award in Orthopedics Research (to A. D.). We also appreciate the generous philanthropic support of William H. and Karen J. Eby and the charitable foundation in their names. The content is solely the responsibility of the authors and does not necessarily represent the official views of the National Institutes of Health.

*Conflict of interest*—A. N. L. receives research support from Zimmer Biomet, Medtronic, and is an unpaid consultant for Globus.

*Abbreviations*—The abbreviations used are: BMP, bone morphogenetic protein; PTH, parathyroid hormone; hBMSCs, human bone marrow–derived mesenchymal stem/stromal cells; $\mu$CT, microcomputed tomography; RPKM, reads per kilobase of transcript per million mapped reads; FC, fold change; DAVID, database for annotation, visualization and integrated discovery; STRING, search tool for the retrieval of interacting genes/proteins; hAMSCs, human adipose–derived mesenchymal/stromal cells; BV/TV, bone volume to total volume ratio; miR, microRNA; RT-qPCR, real-time polymerase chain reaction; H3, histone 3; ANOVA, analysis of variance; PCA, principal component analysis.

## References

1. Chen, D., Zhao, M., and Mundy, G. R. (2004) Bone morphogenetic proteins. *Growth Factors* **22,** 233–241 CrossRef Medline
2. Russow, G., Jahn, D., Appelt, J., Mardian, S., Tsitsilonis, S., and Keller, J. (2018) Anabolic therapies in osteoporosis and bone regeneration. *Int. J. Mol. Sci.* **20,** E83 CrossRef Medline
3. Wozney, J. M., Rosen, V., Celeste, A. J., Mitsock, L. M., Whitters, M. J., Kriz, R. W., Hewick, R. M., and Wang, E. A. (1988) Novel regulators of bone formation: Molecular clones and activities. *Science* **242,** 1528–1534 CrossRef Medline
4. Sampath, T. K., Coughlin, J. E., Whetstone, R. M., Banach, D., Corbett, C., Ridge, R. J., Ozkaynak, E., Oppermann, H., and Rueger, D. C. (1990) Bovine osteogenic protein is composed of dimers of OP-1 and BMP-2A, two members of the transforming growth factor-beta superfamily. *J. Biol. Chem.* **265,** 13198–13205 Medline
5. Shi, Y., and Massagué, J. (2003) Mechanisms of TGF-beta signaling from cell membrane to the nucleus. *Cell* **113,** 685–700 CrossRef Medline
6. Katagiri, T., and Watabe, T. (2016) Bone morphogenetic proteins. *Cold Spring Harb. Perspect. Biol.* **8,** a021899 CrossRef Medline
7. ten Dijke, P., Korchynskyi, O., Valdimarsdottir, G., and Goumans, M. J. (2003) Controlling cell fate by bone morphogenetic protein receptors. *Mol. Cell Endocrinol.* **211,** 105–113 CrossRef Medline
8. Lee, K. S., Kim, H. J., Li, Q. L., Chi, X. Z., Ueta, C., Komori, T., Wozney, J. M., Kim, E. G., Choi, J. Y., Ryoo, H. M., and Bae, S. C. (2000) Runx2 is a common target of transforming growth factor beta1 and bone morphogenetic protein 2, and cooperation between Runx2 and Smad5 induces osteoblast-specific gene expression in the pluripotent mesenchymal precursor cell line C2C12. *Mol. Cell Biol.* **20,** 8783–8792 CrossRef Medline
9. Takazawa, Y., Tsuji, K., Nifuji, A., Kurosawa, H., Ito, Y., and Noda, M. (2000) An osteogenesis-related transcription factor, core-binding factor A1, is constitutively expressed in the chondrocytic cell line TC6, and its expression is upregulated by bone morphogenetic protein-2. *J. Endocrinol.* **165,** 579–586 CrossRef Medline
10. Banerjee, C., Javed, A., Choi, J. Y., Green, J., Rosen, V., van Wijnen, A. J., Stein, J. L., Lian, J. B., and Stein, G. S. (2001) Differential regulation of the two principal Runx2/Cbfa1 n-terminal isoforms in response to bone morphogenetic protein-2 during development of the osteoblast phenotype. *Endocrinology* **142,** 4026–4039 CrossRef Medline
11. Ryoo, H. M., Lee, M. H., and Kim, Y. J. (2006) Critical molecular switches involved in BMP-2-induced osteogenic differentiation of mesenchymal cells. *Gene* **366,** 51–57 CrossRef Medline
12. Lee, M. H., Kim, Y. J., Yoon, W. J., Kim, J. I., Kim, B. G., Hwang, Y. S., Wozney, J. M., Chi, X. Z., Bae, S. C., Choi, K. Y., Cho, J. Y., Choi, J. Y., and Ryoo, H. M. (2005) Dlx5 specifically regulates Runx2 type II expression by binding to homeodomain-response elements in the Runx2 distal promoter. *J. Biol. Chem.* **280,** 35579–35587 CrossRef Medline
13. Ryoo, H. M., Hoffmann, H. M., Beumer, T., Frenkel, B., Towler, D. A., Stein, G. S., Stein, J. L., van Wijnen, A. J., and Lian, J. B. (1997) Stage-specific expression of Dlx-5 during osteoblast differentiation: involvement in regulation of osteocalcin gene expression. *Mol. Endocrinol.* **11,** 1681–1694 CrossRef Medline
14. Nakashima, K., Zhou, X., Kunkel, G., Zhang, Z., Deng, J. M., Behringer, R. R., and de Crombrugghe, B. (2002) The novel zinc finger-containing transcription factor Osterix is required for osteoblast differentiation and bone formation. *Cell* **108,** 17–29 CrossRef Medline
15. Komori, T. (2019) Regulation of proliferation, differentiation and functions of osteoblasts by Runx2. *Int. J. Mol. Sci.* **20,** E1694 CrossRef Medline

16. Einhorn, T. A., and Gerstenfeld, L. C. (2015) Fracture healing: Mechanisms and interventions. *Nat. Rev. Rheumatol.* **11,** 45–54 CrossRef Medline
17. Shapiro, F. (2008) Bone development and its relation to fracture repair. The role of mesenchymal osteoblasts and surface osteoblasts. *Eur. Cell. Mater.* **15,** 53–76 CrossRef Medline
18. Runyan, C. M., and Gabrick, K. S. (2017) Biology of bone formation, fracture healing, and distraction osteogenesis. *J. Craniofac. Surg.* **28,** 1380–1389 CrossRef Medline
19. Tzioupis, C., and Giannoudis, P. V. (2007) Prevalence of long-bone nonunions. *Injury* **38,** Suppl. 2, S3–S9 CrossRef Medline
20. Giannoudis, P. V., Jones, E., and Einhorn, T. A. (2011) Fracture healing and bone repair. *Injury* **42,** 549–550 CrossRef Medline
21. Zura, R., Xiong, Z., Einhorn, T., Watson, J. T., Ostrum, R. F., Prayson, M. J., Della Rocca, G. J., Mehta, S., McKinley, T., Wang, Z., and Steen, R. G. (2016) Epidemiology of fracture nonunion in 18 human bones. *JAMA Surg.* **151,** e162775 CrossRef Medline
22. Hak, D. J., Fitzpatrick, D., Bishop, J. A., Marsh, J. L., Tilp, S., Schnettler, R., Simpson, H., and Alt, V. (2014) Delayed union and nonunions: epidemiology, clinical issues, and financial aspects. *Injury* **45,** Suppl. 2, S3–S7 CrossRef Medline
23. Bostrom, M. P., Lane, J. M., Berberian, W. S., Missri, A. A., Tomin, E., Weiland, A., Doty, S. B., Glaser, D., and Rosen, V. M. (1995) Immunolocalization and expression of bone morphogenetic proteins 2 and 4 in fracture healing. *J. Orthop. Res.* **13,** 357–367 CrossRef Medline
24. Onishi, T., Ishidou, Y., Nagamine, T., Yone, K., Imamura, T., Kato, M., Sampath, T. K., ten Dijke, P., and Sakou, T. (1998) Distinct and overlapping patterns of localization of bone morphogenetic protein (BMP) family members and a BMP type II receptor during fracture healing in rats. *Bone* **22,** 605–612 CrossRef Medline
25. Sciadini, M. F., and Johnson, K. D. (2000) Evaluation of recombinant human bone morphogenetic protein-2 as a bone-graft substitute in a canine segmental defect model. *J. Orthop. Res.* **18,** 289–302 CrossRef Medline
26. Bouxsein, M. L., Turek, T. J., Blake, C. A., D'Augusta, D., Li, X., Stevens, M., Seeherman, H. J., and Wozney, J. M. (2001) Recombinant human bone morphogenetic protein-2 accelerates healing in a rabbit ulnar osteotomy model. *J. Bone Joint Surg. Am.* **83,** 1219–1230 CrossRef Medline
27. Luppen, C. A., Blake, C. A., Ammirati, K. M., Stevens, M. L., Seeherman, H. J., Wozney, J. M., and Bouxsein, M. L. (2002) Recombinant human bone morphogenetic protein-2 enhances osteotomy healing in glucocorticoid-treated rabbits. *J. Bone Miner. Res.* **17,** 301–310 CrossRef Medline
28. Einhorn, T. A., Majeska, R. J., Mohaideen, A., Kagel, E. M., Bouxsein, M. L., Turek, T. J., and Wozney, J. M. (2003) A single percutaneous injection of recombinant human bone morphogenetic protein-2 accelerates fracture repair. *J. Bone Joint Surg. Am.* **85,** 1425–1435 CrossRef Medline
29. Jones, A. L., Bucholz, R. W., Bosse, M. J., Mirza, S. K., Lyon, T. R., Webb, L. X., Pollak, A. N., Golden, J. D., Valentin-Opran, A., and BMP-2 Evaluation in Surgery for Tibial Trauma-Allgraft (BESTT-ALL) Study Group (2006) Recombinant human BMP-2 and allograft compared with autogenous bone graft for reconstruction of diaphyseal tibial fractures with cortical defects. A randomized, controlled trial. *J. Bone Joint Surg. Am.* **88,** 1431–1441 CrossRef Medline
30. Swiontkowski, M. F., Aro, H. T., Donell, S., Esterhai, J. L., Goulet, J., Jones, A., Kregor, P. J., Nordsletten, L., Paiement, G., and Patel, A. (2006) Recombinant human bone morphogenetic protein-2 in open tibial fractures. A subgroup analysis of data combined from two prospective randomized studies. *J. Bone Joint Surg. Am.* **88,** 1258–1265 CrossRef Medline
31. Baskin, D. S., Ryan, P., Sonntag, V., Westmark, R., and Widmayer, M. A. (2003) A prospective, randomized, controlled cervical fusion study using recombinant human bone morphogenetic protein-2 with the CORNERSTONE-SR allograft ring and the ATLANTIS anterior cervical plate. *Spine* **28,** 1219–1224; discussion 1225 CrossRef Medline
32. Ong, K. L., Villarraga, M. L., Lau, E., Carreon, L. Y., Kurtz, S. M., and Glassman, S. D. (2010) Off-label use of bone morphogenetic proteins in the United States using administrative data. *Spine* **35,** 1794–1800 CrossRef Medline
33. Garrison, K. R., Donell, S., Ryder, J., Shemilt, I., Mugford, M., Harvey, I., and Song, F. (2007) Clinical effectiveness and cost-effectiveness of bone morphogenetic proteins in the non-healing of fractures and spinal fusion: A systematic review. *Health Technol. Assess.* **11,** 1–150, iii–iv CrossRef Medline
34. James, A. W., LaChaud, G., Shen, J., Asatrian, G., Nguyen, V., Zhang, X., Ting, K., and Soo, C. (2016) A review of the clinical side effects of bone morphogenetic protein-2. *Tissue Eng. Part B Rev.* **22,** 284–297 CrossRef Medline
35. Gordon, J. A. R., Stein, J. L., Westendorf, J. J., and van Wijnen, A. J. (2015) Chromatin modifiers and histone modifications in bone formation, regeneration, and therapeutic intervention for bone-related disease. *Bone* **81,** 739–745 CrossRef Medline
36. Pike, J. W., Meyer, M. B., St. John, H. C., and Benkusky, N. A. (2015) Epigenetic histone modifications and master regulators as determinants of context dependent nuclear receptor activity in bone cells. *Bone* **81,** 757–764 CrossRef Medline
37. van Wijnen, A. J., and Westendorf, J. J. (2019) Epigenetics as a new frontier in orthopedic regenerative medicine and oncology. *J. Orthop. Res.* **37,** 1465–1474 CrossRef Medline
38. Margueron, R., and Reinberg, D. (2011) The Polycomb complex PRC2 and its mark in life. *Nature* **469,** 343–349 CrossRef Medline
39. Dudakovic, A., and van Wijnen, A. J. (2017) Epigenetic control of osteoblast differentiation by enhancer of zeste homolog 2 (EZH2). *Curr. Mol. Bio. Rep.* **3,** 94–106 CrossRef
40. Margueron, R., Li, G., Sarma, K., Blais, A., Zavadil, J., Woodcock, C. L., Dynlacht, B. D., and Reinberg, D. (2008) Ezh1 and Ezh2 maintain repressive chromatin through different mechanisms. *Mol. Cell* **32,** 503–518 CrossRef Medline
41. Marchesi, I., Giordano, A., and Bagella, L. (2014) Roles of enhancer of zeste homolog 2: From skeletal muscle differentiation to rhabdomyosarcoma carcinogenesis. *Cell Cycle* **13,** 516–527 CrossRef Medline
42. Wyngaarden, L. A., Delgado-Olguin, P., Su, I. H., Bruneau, B. G., and Hopyan, S. (2011) Ezh2 regulates anteroposterior axis specification and proximodistal axis elongation in the developing limb. *Development* **138,** 3759–3767 CrossRef Medline
43. Schwarz, D., Varum, S., Zemke, M., Schöler, A., Baggiolini, A., Draganova, K., Koseki, H., Schübeler, D., and Sommer, L. (2014) Ezh2 is required for neural crest-derived cartilage and bone formation. *Development* **141,** 867–877 CrossRef Medline
44. Dudakovic, A., Camilleri, E. T., Xu, F., Riester, S. M., McGee-Lawrence, M. E., Bradley, E. W., Paradise, C. R., Lewallen, E. A., Thaler, R., Deyle, D. R., Larson, A. N., Lewallen, D. G., Dietz, A. B., Stein, G. S., Montecino, M. A., Westendorf, J. J., and van Wijnen, A. J. (2015) Epigenetic control of skeletal development by the histone methyltransferase Ezh2. *J. Biol. Chem.* **290,** 27604–27617 CrossRef Medline
45. Hemming, S., Cakouros, D., Codrington, J., Vandyke, K., Arthur, A., Zannettino, A., and Gronthos, S. (2017) EZH2 deletion in early mesenchyme compromises postnatal bone microarchitecture and structural integrity and accelerates remodeling. *FASEB J.* **31,** 1011–1027 CrossRef Medline
46. Lui, J. C., Garrison, P., Nguyen, Q., Ad, M., Keembiyehetty, C., Chen, W., Jee, Y. H., Landman, E., Nilsson, O., Barnes, K. M., and Baron, J. (2016) EZH1 and EZH2 promote skeletal growth by repressing inhibitors of chondrocyte proliferation and hypertrophy. *Nat. Commun.* **7,** 13685 CrossRef Medline
47. Dudakovic, A., Camilleri, E. T., Paradise, C. R., Samsonraj, R. M., Gluscevic, M., Paggi, C. A., Begun, D. L., Khani, F., Pichurin, O., Ahmed, F. S., Elsayed, R., Elsalanty, M., McGee-Lawrence, M. E., Karperien, M., Riester, S. M., Thaler, R., Westendorf, J. J., and van Wijnen, A. J. (2018) Enhancer of zeste homolog 2 (Ezh2) controls bone formation and cell cycle progression during osteogenesis in mice. *J. Biol. Chem.* **293,** 12894–12907 CrossRef Medline
48. Camilleri, E. T., Dudakovic, A., Riester, S. M., Galeano-Garces, C., Paradise, C. R., Bradley, E. W., McGee-Lawrence, M. E., Im, H. J., Karperien, M., Krych, A. J., Westendorf, J. J., Larson, A. N., and van Wijnen, A. J. (2018) Loss of histone methyltransferase Ezh2 stimulates an osteogenic transcriptional program in chondrocytes but does not affect cartilage development. *J. Biol. Chem.* **293,** 19001–19011 CrossRef Medline
49. Wei, Y., Chen, Y. H., Li, L. Y., Lang, J., Yeh, S. P., Shi, B., Yang, C. C., Yang, J. Y., Lin, C. Y., Lai, C. C., and Hung, M. C. (2011) CDK1-dependent

phosphorylation of EZH2 suppresses methylation of H3K27 and promotes osteogenic differentiation of human mesenchymal stem cells. *Nat. Cell Biol.* **13,** 87–94 CrossRef Medline

50. Wang, H., Meng, Y., Cui, Q., Qin, F., Yang, H., Chen, Y., Cheng, Y., Shi, J., and Guo, Y. (2016) MiR-101 targets the EZH2/Wnt/β-catenin the pathway to promote the osteogenic differentiation of human bone marrow-derived mesenchymal stem cells. *Sci. Rep.* **6,** 36988 CrossRef Medline
51. Hemming, S., Cakouros, D., Isenmann, S., Cooper, L., Menicanin, D., Zannettino, A., and Gronthos, S. (2014) EZH2 and KDM6A act as an epigenetic switch to regulate mesenchymal stem cell lineage specification. *Stem Cells* **32,** 802–815 CrossRef Medline
52. Zhu, X. X., Yan, Y. W., Chen, D., Ai, C. Z., Lu, X., Xu, S. S., Jiang, S., Zhong, G. S., Chen, D. B., and Jiang, Y. Z. (2016) Long non-coding RNA HoxA-AS3 interacts with EZH2 to regulate lineage commitment of mesenchymal stem cells. *Oncotarget* **7,** 63561–63570 CrossRef Medline
53. Chen, Y. H., Chung, C. C., Liu, Y. C., Yeh, S. P., Hsu, J. L., Hung, M. C., Su, H. L., and Li, L. Y. (2016) Enhancer of zeste homolog 2 and histone deacetylase 9c regulate age-dependent mesenchymal stem cell differentiation into osteoblasts and adipocytes. *Stem Cells* **34,** 2183–2193 CrossRef Medline
54. Dudakovic, A., Camilleri, E. T., Riester, S. M., Paradise, C. R., Gluscevic, M., O'Toole, T. M., Thaler, R., Evans, J. M., Yan, H., Subramaniam, M., Hawse, J. R., Stein, G. S., Montecino, M. A., McGee-Lawrence, M. E., Westendorf, J. J., and van Wijnen, A. J. (2016) Enhancer of zeste homolog 2 inhibition stimulates bone formation and mitigates bone loss caused by ovariectomy in skeletally mature mice. *J. Biol. Chem.* **291,** 24594–24606 CrossRef Medline
55. Jing, H., Liao, L., An, Y., Su, X., Liu, S., Shuai, Y., Zhang, X., and Jin, Y. (2016) Suppression of EZH2 prevents the shift of osteoporotic MSC fate to adipocyte and enhances bone formation during osteoporosis. *Mol. Ther.* **24,** 217–229 CrossRef Medline
56. Fang, C., Qiao, Y., Mun, S. H., Lee, M. J., Murata, K., Bae, S., Zhao, B., Park-Min, K. H., and Ivashkiv, L. B. (2016) Cutting edge: EZH2 promotes osteoclastogenesis by epigenetic silencing of the negative regulator IRF8. *J. Immunol.* **196,** 4452–4456 CrossRef Medline
57. Woodhouse, S., Pugazhendhi, D., Brien, P., and Pell, J. M. (2013) Ezh2 maintains a key phase of muscle satellite cell expansion but does not regulate terminal differentiation. *J. Cell Sci.* **126,** 565–579 CrossRef Medline
58. Kim, K. H., and Roberts, C. W. (2016) Targeting EZH2 in cancer. *Nat. Med.* **22,** 128–134 CrossRef Medline
59. Comet, I., Riising, E. M., Leblanc, B., and Helin, K. (2016) Maintaining cell identity: PRC2-mediated regulation of transcription and cancer. *Nat. Rev. Cancer* **16,** 803–810 CrossRef Medline
60. Metsalu, T., and Vilo, J. (2015) ClustVis: A web tool for visualizing clustering of multivariate data using Principal Component Analysis and heatmap. *Nucleic Acids Res.* **43,** W566–W570 CrossRef Medline
61. Hassan, M. Q., Javed, A., Morasso, M. I., Karlin, J., Montecino, M., van Wijnen, A. J., Stein, G. S., Stein, J. L., and Lian, J. B. (2004) Dlx3 transcriptional regulation of osteoblast differentiation: Temporal recruitment of Msx2, Dlx3, and Dlx5 homeodomain proteins to chromatin of the osteocalcin gene. *Mol. Cell Biol.* **24,** 9248–9261 CrossRef Medline
62. Samsonraj, R. M., Paradise, C. R., Dudakovic, A., Sen, B., Nair, A. A., Dietz, A. B., Deyle, D. R., Cool, S. M., Rubin, J., and van Wijnen, A. J. (2018) Validation of osteogenic properties of cytochalasin D by high-resolution RNA-sequencing in mesenchymal stem cells derived from bone marrow and adipose tissues. *Stem Cells Dev.* **27,** 1136–1145 CrossRef Medline
63. Samsonraj, R. M., Dudakovic, A., Zan, P., Pichurin, O., Cool, S. M., and van Wijnen, A. J. (2017) A versatile protocol for studying calvarial bone defect healing in a mouse model. *Tissue Eng. Part C Methods* **23,** 686–693 CrossRef Medline
64. Spicer, P. P., Kretlow, J. D., Young, S., Jansen, J. A., Kasper, F. K., and Mikos, A. G. (2012) Evaluation of bone regeneration using the rat critical size calvarial defect. *Nat. Protoc.* **7,** 1918–1929 CrossRef Medline
65. Ge, K. (2012) Epigenetic regulation of adipogenesis by histone methylation. *Biochim. Biophys. Acta* **1819,** 727–732 CrossRef Medline
66. Wang, E. A., Rosen, V., Cordes, P., Hewick, R. M., Kriz, M. J., Luxenberg, D. P., Sibley, B. S., and Wozney, J. M. (1988) Purification and characterization of other distinct bone-inducing factors. *Proc. Natl. Acad. Sci. U.S.A.* **85,** 9484–9488 CrossRef Medline
67. Katagiri, T., Yamaguchi, A., Ikeda, T., Yoshiki, S., Wozney, J. M., Rosen, V., Wang, E. A., Tanaka, H., Omura, S., and Suda, T. (1990) The non-osteogenic mouse pluripotent cell line, C3H10T1/2, is induced to differentiate into osteoblastic cells by recombinant human bone morphogenetic protein-2. *Biochem. Biophys. Res. Commun.* **172,** 295–299 CrossRef Medline
68. Yamaguchi, A., Katagiri, T., Ikeda, T., Wozney, J. M., Rosen, V., Wang, E. A., Kahn, A. J., Suda, T., and Yoshiki, S. (1991) Recombinant human bone morphogenetic protein-2 stimulates osteoblastic maturation and inhibits myogenic differentiation in vitro. *J. Cell Biol.* **113,** 681–687 CrossRef Medline
69. Lee, Z. H., Kim, H. J., and Ryoo, H. M. (2015) A novel osteogenic activity of suberoylanilide hydroxamic acid is synergized by BMP-2. *J. Bone Metabol.* **22,** 51–56 CrossRef Medline
70. Cho, Y. D., Yoon, W. J., Kim, W. J., Woo, K. M., Baek, J. H., Lee, G., Ku, Y., van Wijnen, A. J., and Ryoo, H. M. (2014) Epigenetic modifications and canonical wingless/int-1 class (WNT) signaling enable trans-differentiation of nonosteogenic cells into osteoblasts. *J. Biol. Chem.* **289,** 20120–20128 CrossRef Medline
71. Gao, S., Wang, Z., Wang, W., Hu, X., Chen, P., Li, J., Feng, X., Wong, J., and Du, J. X. (2017) The lysine methyltransferase SMYD2 methylates the kinase domain of type II receptor BMPR2 and stimulates bone morphogenetic protein signaling. *J. Biol. Chem.* **292,** 12702–12712 CrossRef Medline
72. Sun, J., Ermann, J., Niu, N., Yan, G., Yang, Y., Shi, Y., and Zou, W. (2018) Histone demethylase LSD1 regulates bone mass by controlling WNT7B and BMP2 signaling in osteoblasts. *Bone Res.* **6,** 14 CrossRef Medline
73. Hay, E., Hott, M., Graulet, A. M., Lomri, A., and Marie, P. J. (1999) Effects of bone morphogenetic protein-2 on human neonatal calvaria cell differentiation. *J. Cell Biochem.* **72,** 81–93 CrossRef Medline
74. Huang, W., Rudkin, G. H., Carlsen, B., Ishida, K., Ghasri, P., Anvar, B., Yamaguchi, D. T., and Miller, T. A. (2002) Overexpression of BMP-2 modulates morphology, growth, and gene expression in osteoblastic cells. *Exp. Cell Res.* **274,** 226–234 CrossRef Medline
75. Phimphilai, M., Zhao, Z., Boules, H., Roca, H., and Franceschi, R. T. (2006) BMP signaling is required for RUNX2-dependent induction of the osteoblast phenotype. *J. Bone Miner. Res.* **21,** 637–646 CrossRef Medline
76. Javed, A., Afzal, F., Bae, J. S., Gutierrez, S., Zaidi, K., Pratap, J., van Wijnen, A. J., Stein, J. L., Stein, G. S., and Lian, J. B. (2009) Specific residues of RUNX2 are obligatory for formation of BMP2-induced RUNX2-SMAD complex to promote osteoblast differentiation. *Cells Tissues Organs* **189,** 133–137 CrossRef Medline
77. Lee, M. H., Kim, Y. J., Kim, H. J., Park, H. D., Kang, A. R., Kyung, H. M., Sung, J. H., Wozney, J. M., Kim, H. J., and Ryoo, H. M. (2003) BMP-2-induced Runx2 expression is mediated by Dlx5, and TGF-beta 1 opposes the BMP-2-induced osteoblast differentiation by suppression of Dlx5 expression. *J. Biol. Chem.* **278,** 34387–34394 CrossRef Medline
78. Javed, A., Gutierrez, S., Montecino, M., van Wijnen, A. J., Stein, J. L., Stein, G. S., and Lian, J. B. (1999) Multiple Cbfa/AML sites in the rat osteocalcin promoter are required for basal and vitamin D-responsive transcription and contribute to chromatin organization. *Mol. Cell Biol.* **19,** 7491–7500 CrossRef Medline
79. Matsubara, T., Kida, K., Yamaguchi, A., Hata, K., Ichida, F., Meguro, H., Aburatani, H., Nishimura, R., and Yoneda, T. (2008) BMP2 regulates Osterix through Msx2 and Runx2 during osteoblast differentiation. *J. Biol. Chem.* **283,** 29119–29125 CrossRef Medline
80. Cho, Y. D., Kim, W. J., Yoon, W. J., Woo, K. M., Baek, J. H., Lee, G., Kim, G. S., and Ryoo, H. M. (2012) Wnt3a stimulates Mepe, matrix extracellular phosphoglycoprotein, expression directly by the activation of the canonical Wnt signaling pathway and indirectly through the stimulation of autocrine Bmp-2 expression. *J. Cell Physiol.* **227,** 2287–2296 CrossRef Medline
81. Lu, Z., Wang, G., Dunstan, C. R., and Zreiqat, H. (2012) Short-term exposure to tumor necrosis factor-α enables human osteoblasts to direct adipose tissue-derived mesenchymal stem cells into osteogenic differentiation. *Stem Cells Dev.* **21,** 2420–2429 CrossRef Medline
82. Scandura, J. M., Roboz, G. J., Moh, M., Morawa, E., Brenet, F., Bose, J. R., Villegas, L., Gergis, U. S., Mayer, S. A., Ippoliti, C. M., Curcio, T. J., Ritchie, E. K., and Feldman, E. J. (2011) Phase 1 study of epigenetic priming with

decitabine prior to standard induction chemotherapy for patients with AML. *Blood* **118,** 1472–1480 CrossRef Medline

83. Vicente-Dueñas, C., Hauer, J., Cobaleda, C., Borkhardt, A., and Sánchez-García, I. (2018) Epigenetic priming in cancer initiation. *Trends Cancer* **4,** 408–417 CrossRef Medline
84. Auh, Q. S., Park, K. R., Yun, H. M., Lim, H. C., Kim, G. H., Lee, D. S., Kim, Y. C., Oh, H., and Kim, E. C. (2016) Sulfuretin promotes osteoblastic differentiation in primary cultured osteoblasts and *in vivo* bone healing. *Oncotarget* **7,** 78320–78330 CrossRef Medline
85. Herberg, S., Aguilar-Perez, A., Howie, R. N., Kondrikova, G., Periyasamy-Thandavan, S., Elsalanty, M. E., Shi, X., Hill, W. D., and Cray, J. J. (2017) Mesenchymal stem cell expression of SDF-1$\beta$ synergizes with BMP-2 to augment cell-mediated healing of critical-sized mouse calvarial defects. *J. Tissue Eng. Regen. Med.* **11,** 1806–1819 CrossRef Medline
86. Reyes, R., Rodríguez, J. A., Orbe, J., Arnau, M. R., Évora, C., and Delgado, A. (2018) Combined sustained release of BMP2 and MMP10 accelerates bone formation and mineralization of calvaria critical size defect in mice. *Drug Delivery* **25,** 750–756 CrossRef Medline
87. Liao, Y. H., Chang, Y. H., Sung, L. Y., Li, K. C., Yeh, C. L., Yen, T. C., Hwang, S. M., Lin, K. J., and Hu, Y. C. (2014) Osteogenic differentiation of adipose-derived stem cells and calvarial defect repair using baculovirus-mediated co-expression of BMP-2 and miR-148b. *Biomaterials* **35,** 4901–4910 CrossRef Medline
88. Li, K. C., Lo, S. C., Sung, L. Y., Liao, Y. H., Chang, Y. H., and Hu, Y. C. (2017) Improved calvarial bone repair by hASCs engineered with Cre/loxP-based baculovirus conferring prolonged BMP-2 and MiR-148b co-expression. *J. Tissue Eng. Regen. Med.* **11,** 3068–3077 CrossRef Medline
89. Wang, D., Christensen, K., Chawla, K., Xiao, G., Krebsbach, P. H., and Franceschi, R. T. (1999) Isolation and characterization of MC3T3-E1 preosteoblast subclones with distinct in vitro and in vivo differentiation/mineralization potential. *J. Bone Miner. Res.* **14,** 893–903 CrossRef Medline
90. Schneider, C. A., Rasband, W. S., and Eliceiri, K. W. (2012) NIH Image to ImageJ: 25 years of image analysis. *Nat. Methods* **9,** 671–675 CrossRef Medline
91. Villanueva, A. R., and Mehr, L. A. (1977) Modifications of the Goldner and Gomori one-step trichrome stains for plastic-embedded thin sections of bone. *Am. J. Med. Technol.* **43,** 536–538 Medline
92. Dudakovic, A., Camilleri, E., Riester, S. M., Lewallen, E. A., Kvasha, S., Chen, X., Radel, D. J., Anderson, J. M., Nair, A. A., Evans, J. M., Krych, A. J., Smith, J., Deyle, D. R., Stein, J. L., Stein, G. S., Im, H. J., Cool, S. M., Westendorf, J. J., Kakar, S., Dietz, A. B., and van Wijnen, A. J. (2014) High-resolution molecular validation of self-renewal and spontaneous differentiation in clinical-grade adipose-tissue derived human mesenchymal stem cells. *J. Cell Biochem.* **115,** 1816–1828 CrossRef Medline
93. Dudakovic, A., Gluscevic, M., Paradise, C. R., Dudakovic, H., Khani, F., Thaler, R., Ahmed, F. S., Li, X., Dietz, A. B., Stein, G. S., Montecino, M. A., Deyle, D. R., Westendorf, J. J., and van Wijnen, A. J. (2017) Profiling of human epigenetic regulators using a semi-automated real-time qPCR platform validated by next generation sequencing. *Gene* **609,** 28–37 CrossRef Medline
94. Huang, D. W, Sherman, B. T., and Lempicki, R. A. (2009) Bioinformatics enrichment tools: Paths toward the comprehensive functional analysis of large gene lists. *Nucleic Acids Res.* **37,** 1–13 CrossRef Medline
95. Huang da, W, Sherman, B. T., and Lempicki, R. A. (2009) Systematic and integrative analysis of large gene lists using DAVID bioinformatics resources. *Nat. Protoc.* **4,** 44–57 CrossRef Medline
96. Szklarczyk, D., Gable, A. L., Lyon, D., Junge, A., Wyder, S., Huerta-Cepas, J., Simonovic, M., Doncheva, N. T., Morris, J. H., Bork, P., Jensen, L. J., and Mering, C. V. (2019) STRING v11: Protein-protein association networks with increased coverage, supporting functional discovery in genome-wide experimental datasets. *Nucleic Acids Res.* **47,** D607–D613 CrossRef Medline
97. Ramírez, F., Ryan, D. P., Grüning, B., Bhardwaj, V., Kilpert, F., Richter, A. S., Heyne, S., Dündar, F., and Manke, T. (2016) deepTools2: A next generation web server for deep-sequencing data analysis. *Nucleic Acids Res.* **44,** W160–W165 CrossRef Medline
98. Dudakovic, A., and van Wijen, A. J. (2016) Ezh2 Inhibition is bone-anabolic and osteoprotective in skeletally mature mice. Gene Expression Omnibus. GSE83506